

1
2
3
4 **1 Multiple episodes of gold mineralization in the East Kunlun Orogen, western Central**
5
6 **2 Orogenic Belt, China: Constraints from Re-Os sulfide geochronology**
7
8

9
10
11 **3**
12 **4 Jiajie Chen^{1,2,3} · Lebing Fu² · David Selby³ · Junhao Wei² · Xu Zhao² · Hongzhi Zhou²**
13

14
15
16
17 **6** ¹ State Key Laboratory of Nuclear Resources and Environment, School of Earth Sciences,
18
19 **7** East China University of Technology, Nanchang, 330013, China
20

21
22 **8** ² Faculty of Earth Resources, China University of Geosciences, Wuhan, 430074, China
23

24
25 **9** ³ Department of Earth Sciences, University of Durham, Durham, DH1 3LE, UK
26

27
28
29 **11** ✉ Junhao Wei
30

31
32 **12** E-mail: junhaow@163.com
33

34
35 **13** Tel: +86-13437179812.
36
37
38
39
40
41
42
43
44
45
46
47
48
49
50
51
52
53
54
55
56
57
58
59

60
61
62
63 **Abstract**
64

65 15 The Gouli goldfield (>110 t Au), located in the East Kunlun Orogen, western Central
66
67
68 16 Orogenic Belt of China, is one of the most important goldfields in this area. In the last
69
70
71 17 decade, a number of orogenic gold deposits (e.g., Guoluolongwa and Annage) have been
72
73 18 shown to be hosted by rock units of different lithology and ages. Rhenium-osmium (Re-Os)
74
75
76 19 geochronology of sulfides from gold-bearing veins was performed to define the chronologic
77
78 20 relationships between gold mineralization present in the metamorphic rocks (Proterozoic and
79
80
81 21 Silurian) of the East Kunlun Orogen. Sulfides (pyrite and chalcopyrite) from pyrite-quartz
82
83 22 vein and polymetallic sulfides-quartz vein in the Guoluolongwa gold deposit yield Re-Os
84
85
86 23 isochron dates of 374 ± 15 Ma (MSWD = 4.6; initial $^{187}\text{Os}/^{188}\text{Os}$ ratio (Osi) = 0.06 ± 0.22)
87
88 24 and 354 ± 7 Ma (MSWD = 0.18; Osi = 0.13 ± 0.01), respectively. Similar ages are also
89
90
91 25 revealed by the pyrite mineral separates from the Annage gold deposit (383 ± 8 Ma and $349 \pm$
92
93 26 6 Ma). These ages are interpreted to record the timings of the formation of the two vein types
94
95
96 27 in these deposits, which are nominally separated by ~20 Ma.

97
98 28 The new Re-Os ages presented here identify the first two Late Paleozoic (Devonian and
99
100 29 Early Carboniferous) gold-mineralizing events in the East Kunlun Orogen and thus indicate
101
102
103 30 at least two mineralization epochs in this area given ages (Late Triassic) of other gold
104
105
106 31 systems and field observations. Considering the geological background and temporal
107
108 32 distribution of gold deposits in adjacent areas (western Qinling and Qaidam-Qilian), we
109
110
111 33 suggest that gold deposits in the western Central Orogenic Belt were formed in
112
113 34 collisional/post-collisional settings being controlled by common tectonic-magmatic activities
114
115
116
117
118

119
120
121
122 35 related to the evolution of both the Prototethys Ocean (Proterozoic – Paleozoic) and
123
124 36 Paleotethys Ocean (Paleozoic – Early Cenozoic).

125
126
127 37 Further, the initial Os (O_{Si}) obtained from the Re-Os isochron suggest that for the two vein
128
129 38 types in the Guoluolongwa gold deposit the Os and by inference the ore metal (Au) were
130
131 39 derived from a mantle-like source (O_{Si} values = $\sim 0.12 - 0.13$), which should be related to the
132
133 40 contemporaneous mantle-like magmatism. In contrast, the pyrite-quartz vein in the Annage
134
135 41 gold deposit possesses a significantly radiogenic O_{Si} value (3.65 ± 0.51). Given the similar
136
137 42 timing of mineralization between the Guoluolongwa and Annage deposits, it is considered
138
139 43 that the ore metal likely has a similar origin, i.e., a mantle-like source, however at Annage the
140
141 44 hydrothermal fluid interacted with the Proterozoic metamorphic host rocks and leached
142
143 45 radiogenic Os that masks any evidence of a mantle-like source.
144
145
146
147
148
149

150 46

151
152 47 Keywords: Gold deposit; Paleozoic mineralization; Re-Os isotopic dating; East Kunlun
153
154 48 Orogen
155
156
157
158
159
160
161
162
163
164
165
166
167
168
169
170
171
172
173
174
175
176
177

178
179
180
181 **49 1. Introduction**
182

183
184 50 The East Kunlun Orogen, comprising the western part of the Central Orogenic Belt of China
185
186 51 (Fig. 1A), records two stages of orogenesis that correspond to the evolution of the
187
188
189 52 Neoproterozoic–Late Paleozoic Prototethys Ocean and Late Paleozoic–Triassic Paleotethys
190
191 53 Ocean in this area (Fig. 1B; Ma et al., 2015). During the last ten years, in the East Kunlun
192
193
194 54 Orogen, a number of gold deposits/fields, such as the Wulonggou (>70 t Au; unpublished
195
196 55 report; Zhang et al., 2017) and Gouli (>110 t Au; unpublished report) goldfields, and the
197
198
199 56 Balong and Kaihuangbei gold deposits, have been discovered (Fig.1C; Zhao, 2004 and
200
201 57 references therein). Most of the gold deposits/fields exhibit quartz-vein type or fracture-
202
203
204 58 hosted pervasive alteration type mineralization and are spatially controlled by brittle-ductile
205
206
207 59 shear zones and, in turn, have been regarded to be orogenic gold deposits (Feng, 2002; Zhao,
208
209 60 2004). A Silurian–Devonian timing, coincident with that of the evolution of Prototethys, has
210
211 61 been proposed to be responsible for the formation of these deposits based on the conclusion
212
213
214 62 that the ore-controlling structures were formed during the Silurian-Devonian tectonic
215
216
217 63 deformation (e.g., Zhang et al., 2001; Feng, 2002 and references therein). However, reported
218
219 64 Ar-Ar dating of sericite or muscovite from gold deposits in the East Kunlun Orogen revealed
220
221 65 a Triassic age population (Feng, 2002; Zhao, 2004; Zhang et al., 2005; Xiao et al., 2014;
222
223
224 66 Zhang et al., 2017). This, together with the close spatial relationship between some gold
225
226
227 67 deposits and ubiquitous Late Permian-Triassic granitoids (Li et al., 2012; Zhang et al., 2017)
228
229 68 is taken to suggest that the Triassic gold-mineralizing dominated the formation of these
230
231 69 deposits, although the gold deposits in this area are hosted by different geological units of
232
233
234
235
236

237
238
239
240
241
242
243
244
245
246
247
248
249
250
251
252
253
254
255
256
257
258
259
260
261
262
263
264
265
266
267
268
269
270
271
272
273
274
275
276
277
278
279
280
281
282
283
284
285
286
287
288
289
290
291
292
293
294
295

70 various ages (from Paleozoic to Mesozoic). The lack of a temporal record of Paleozoic “gold
71 mineralization” may be due to: (1) an early Paleozoic mineralization event did not occur, and
72 (2) post-ore thermal events, such as Triassic mineralization or extensive magmatism, have
73 reset the Ar-Ar systems in micaceous minerals due to the susceptibility of this system to
74 hydrothermal overprint (Selby et al., 2002). The ambiguity of the timing of the early and late
75 “gold-mineralizing events” not only hampers our understanding of the origin of these gold
76 deposits but also exploration. As such, a more robust dating method is required.

77 Recently, rhenium-osmium (Re-Os) isotopic dating of sulfide minerals (e.g., pyrite,
78 chalcopyrite, and molybdenite) has been applied to several types of hydrothermal deposits.
79 Among these sulfide minerals, molybdenite is particularly suitable for Re-Os geochronology,
80 given its high abundance of Re (typically ppm levels) and negligible common Os (Stein et al.,
81 2003; Selby and Creaser, 2004). However, molybdenite is commonly absent in many gold
82 deposits, nevertheless other sulfides, e.g. pyrite (Stein et al., 2000), arsenopyrite (Morelli et
83 al., 2005; Morelli et al., 2007), chalcopyrite (Lawley et al., 2013), bornite (Selby et al., 2009)
84 and even pyrrhotite (Wang et al., 2008) can be utilized to delineate the timing of gold
85 mineralization. In this contribution, we present Re-Os geochronology on gold-related pyrite
86 and chalcopyrite from two deposits in the Gouli goldfield located in the eastern East Kunlun
87 Orogen, western Central Orogenic Belt to pinpoint the timing of gold mineralization and
88 constrain the sources of ore-forming materials. We demonstrate that at least two gold
89 mineralizing epochs (Late Paleozoic and Late Triassic) exist in the East Kunlun Orogen and

296
297
298
299 90 possibly wider west of Central Orogenic Belt and that the ore metal (Au) exhibit a mantle-
300
301 like derived origin.
302 91
303

304 92 **2. Regional and deposit geology**

306 93 The East Kunlun Orogen is located in the northern Tibet and is bounded by the Qaidam Basin
307
308 94 to the north, the Qinling Orogen to the east, the Bayan Har Terrane to the south and the Altyn
309
310 Tagh fault to the west (Fig. 1B). The East Kunlun Orogen is composed of the Northern East
311
312 95 Kunlun Terrane and the Southern East Kunlun Terrane, which are separated by the Central
313
314 96 East Kunlun Suture Zone (Fig. 1C). Two regional suture zones, the Central East Kunlun
315
316 97 Suture Zone and Southern East Kunlun Suture Zone, which correspond to the evolution of the
317
318 98 Prototethys Ocean (Proterozoic–Early Paleozoic) and Paleotethys Ocean (Late Paleozoic –
319
320 99 Mesozoic), respectively, traverse the East Kunlun Orogen (e.g., Yang et al., 1996). The
321
322 100 basement rocks in the East Kunlun Orogen are composed of Proterozoic intermediate – high -
323
324 101 grade metamorphic rocks that are mainly exposed in the Northern East Kunlun Terrane
325
326 102 (Meng et al., 2013; He et al., 2016; Wei et al., 2016). Overlying these basement rocks are the
327
328 103 Early Paleozoic low-grade metamorphic sedimentary and volcanic rocks (e.g., Chen et al.,
329
330 104 2013; Chen et al., 2014) that are unconformably overlain by the Devonian Maoniushan
331
332 105 Formation (molasse) (e.g., Zhang et al., 2010). Carboniferous–Middle Triassic marine facies
333
334 106 rocks mainly occur in the Southern East Kunlun Terrane. Magmatic rocks in the East Kunlun
335
336 107 Orogen consist of granitoids with minor mafic-ultramafic rocks (Fig. 1C). The mafic-
337
338 108 ultramafic rocks occur mainly along the Central East Kunlun Suture Zone and Southern East
339
340 109 Kunlun Suture Zone. The mafic-ultramafic rocks from the Central East Kunlun Suture Zone
341
342 110
343
344
345
346
347
348
349
350
351
352
353
354

355
356
357
358 111 are dated as Cambrian-Ordovician with ages that range from 537 Ma to 467 Ma (Zhu et al.,
359
360 112 2000; Bian et al., 2004; Li et al., 2013; Wei, 2015; Qi et al., 2016). The mafic-ultramafic
362
363 113 units from the Southern East Kunlun Suture Zone exhibit both Cambrian-Ordovician (555–
364
365 114 516 Ma; Li, 2008; Liu et al., 2011) and Carboniferous ages (345–332 Ma; Chen et al., 2001;
366
367
368 115 Liu et al., 2011). The granitoids yield dates mainly concentrated in Ordovician-Devonian
369
370
371 116 (470–390 Ma) and Permian-Triassic (260–220 Ma) (Mo et al., 2007). Granitoids in both age
372
373 117 groups show time-varying lithology from early calc-alkaline granodiorites to late
374
375
376 118 monzogranites and syenogranites (e.g., Lu et al., 2013; Zhang et al., 2014; Chen et al., 2016;
377
378 119 Chen et al., 2017). Succeeding the Ordovician-Devonian massive intrusion of granitoids were
379
380
381 120 widespread volcanic activities, which are evidenced by bimodal volcanic rocks from the
382
383 121 Maoniushan Formation (Zhang et al., 2010; Liu et al., 2016).

385 122 *2.1 Geology of the Gouli goldfield*

388 123 The Gouli goldfield is located in the east end of the East Kunlun Orogen (Fig. 1C). The
389
390
391 124 Central East Kunlun Suture Zone, which is evidenced by the ophiolites, traverses the central
392
393 125 part of this area (Fig. 2). Proterozoic middle–high-grade metamorphic basement rocks occur
394
395
396 126 across the entire area. Overlying the basement rocks are the Ordovician-Silurian low-grade
397
398 127 metamorphic rocks from the Naj Tai Group, Devonian Maoniushan Formation and the
399
400
401 128 Carboniferous–Triassic sedimentary and volcanic rocks. The lithology of magmatic rocks
402
403 129 varies from mafic-ultramafic intrusions/dikes to felsic granitoids. The mafic-ultramafic rocks
404
405
406 130 exhibit Cambrian and Devonian-Carboniferous ages (Yang et al., 1996; Chen et al., 2001;
407
408 131 Feng et al., 2010), with the felsic granitoids mainly defining two age groups, Ordovician-

414
415
416
417 132 Devonian and Permian-Triassic (Fig. 2). A number of gold deposits have been discovered in
418
419
420 133 this field, including the Guoluolongwa (>40 t Au), Annage (>8 t Au), Asiha (>6 t Au),
421
422 134 Walega (>12 t Au) and Delong (>5 t Au) (unpublished report). These deposits can be divided
423
424
425 135 into two groups according to their host rocks, ore-controlling structure, mineralization styles,
426
427 136 and alteration. Group one, represented by the Guoluolongwa and Annage, is hosted in
428
429
430 137 metamorphic rocks (Proterozoic for Annage and Silurian for Guoluolongwa) (Figs 2–4;
431
432 138 Ding et al., 2013; Tao, 2014), mainly controlled by EW-trending brittle-ductile shear zone,
433
434
435 139 which contrast to the Group two deposits (represented by the Walega and Asiha) being hosted
436
437 140 in Silurian (Fig. 2; 431–440 Ma; our unpublished data) or Triassic (238–244 Ma; Fig. 2; Li et
438
439
440 141 al., 2012; Li et al., 2014) felsic intrusions and mainly controlled by NW or NE-trending
441
442 142 brittle fractures (Chen, 2018). The gold mineralization of both groups is mainly associated
443
444
445 143 with quartz veins and subordinate associated with pervasively altered fracture zones.
446
447 144 However, the mineral assemblages of the two groups are distinct, with group one showing
448
449
450 145 sulfides dominated by pyrite and those of group two dominated by arsenopyrite (Chen, 2018).
451
452 146 The close spatial relationship of these deposits makes researchers consider that these deposits
453
454
455 147 were formed by a common mineralization event during Triassic after the emplacement of the
456
457 148 youngest host (Asiha quartz diorite) (Yue, 2013).

460 149 *2.2 Geology of the Guoluolongwa and Annage gold deposits*

462 150 In the Central East Kunlun Suture Zone, the Guoluolongwa gold deposit is the largest gold
463
464
465 151 deposit in the Gouli goldfield. The ore deposit is structurally controlled by the Silurian–
466
467 152 Devonian formed (427–408 Ma; Wang et al., 2003), EW-trending thrust zone. In the north of
468
469
470
471
472

473
474
475
476 153 the deposit is the oldest rock unit, Proterozoic aged schist (Fig. 3). In the center of the deposit
477
478
479 154 are the Ordovician-Silurian Najj Tal Group metamorphic rocks, which have zircon U-Pb ages
480
481 155 of 479.1 ± 2.4 and 479.7 ± 5.6 Ma, indicating that the sedimentary and volcanic protoliths
482
483
484 156 were formed no later than 479 Ma. (Fig. 3A; our unpublished data). In the south of the
485
486 157 deposit are conglomerates of the Devonian Maoniushan Formation (e.g., Lu et al., 2010).
487
488 158 Magmatic rocks in this area include mylonitic diorite (~ 477 Ma; our unpublished data) and
489
490
491 159 gabbro (416 Ma; Yue et al., 2013).

492
493
494 160 Six gold orebodies (I – VI) have been delineated in the Guoluolongwa gold system (Fig.
495
496 161 3). All of the orebodies show an EW trend (Fig. 3A) and high angle dips ($50 - 80^\circ$) towards
497
498
499 162 the south (180° ; Fig. 3B). The gold grades vary from 1 g/t to hundreds g/t, with an average
500
501 163 grade at 6.75 g/t (Fig. 3B; unpublished geological report). The gold mineralization is mainly
502
503
504 164 associated with quartz veins that cross cut the Devonian gabbro (Yue et al., 2013), with
505
506 165 subordinate pervasively altered fracture-hosted mineralization occurring in the north of the
507
508
509 166 deposit area (Xiao et al., 2014).

510
511 167 Three stages of mineralization are defined at the Guoluolongwa based on mineral
512
513
514 168 assemblages and crosscutting relationships (Figs. 5–6). The first stage is characterized by
515
516 169 coarse milky quartz with sparse coarse pyrite (up to 5 mm) (stage I vein), which is cross-cut
517
518
519 170 by the disseminated-massive pyrite-quartz vein of the second stage (stage II vein). Both
520
521 171 coarse and fine grain pyrite can be observed in the stage II vein (Fig. 5H) that are cut cross
522
523
524 172 by the polymetallic stage III quartz vein (Figs. 5D and H). Minerals in the stage III quartz
525
526 173 vein mainly include pyrite, sphalerite, galena, chalcopyrite and quartz (Figs. 5D and I).
527
528
529
530
531

532
533
534
535 174 Native gold can be found in fractures of pyrite and between grains of sulfide and quartz (Figs.
536
537 175 5D and E) or as inclusions enwrapped in pyrite and quartz (Yang et al., 2006). High-grade
538
539
540 176 gold ores are found associated with both stage II and III veins.

541
542 177 The Annage gold deposit is located to the immediate northwest (<3km) of the
543
544
545 178 Guoluolongwa deposit (Fig. 2). As such the local geology is very similar to that of the
546
547
548 179 Guoluolongwa deposit. But in contrast, the ore bodies are hosted by Proterozoic metamorphic
549
550 180 mica-quartz schist, amphibolite and marble units (Fig. 4). Most of the Annage orebodies (I,
551
552
553 181 II, V, and VI; Fig. 4) strike east-west and dip 50 – 85° to south-southwest (Fig. 4). The
554
555 182 orebodies as a whole show identical mineralization stages and mineral assemblages to those
556
557
558 183 of the Guoluolongwa system (Chen, 2014; Tao, 2014), suggesting that the two gold deposits
559
560 184 should have a common origin. However, some orebodies at Annage (e.g., orebody I; Figs. 4
561
562
563 185 and 5J-I) are dominated by stage II vein (gold grade averaging at 5.18 g/t) with the stage III
564
565 186 polymetallic sulfides-quartz vein mineralization poorly developed. The ore grades vary
566
567
568 187 widely (grades of different ore bodies average between 1.06 and 43.51 g/t), with the highest
569
570 188 grade being 156 g/t.

571 572 189 **3. Sampling and analytical methods**

573
574
575 190 To define the timing of sulfide (\pm gold) mineralization by application of the Re-Os
576
577
578 191 chronometer, fourteen samples from the quartz vein orebodies (seven from the stage II veins
579
580 192 and seven from the stage III veins) of the Guoluolongwa system and 10 samples from the
581
582
583 193 pyrite-quartz veins (orebody I; Fig. 5E) of the Annage gold deposit were selected. For the
584
585 194 Guoluolongwa system, samples are all collected from the underground tunnel of orebodies I
586
587
588
589
590

591
592
593
594 195 and VI (Fig. 3). Samples for the stage II quartz veins were collected from the massive or
595
596 196 veinlet ores (Figs. 5A and B), both of which crosscut the stage I milky quartz veins. Samples
597
598
599 197 for the stage III quartz veins were collected from dense disseminated ores that are mainly
600
601
602 198 composed of galena, sphalerite, chalcopyrite, pyrite and quartz (Fig. 5C). In total, seven
603
604 199 pyrite mineral separates from the stage II veins, and four pyrite and three chalcopyrite
605
606
607 200 mineral separates from the stage III veins were prepared for the Guoluolongwa gold deposit.
608
609 201 For the Annage deposit, the samples were all collected from the open mining pit of orebody I
610
611
612 202 (Fig. 4) that is mainly composed of Stage II pyrite-quartz vein (Figs. 5J and K). In total, ten
613
614 203 pyrite mineral separates were prepared. The mineral separates were obtained using traditional
615
616
617 204 isolation methods (e.g., crushing, heavy liquids separation and handpicking).

618
619 205 The Re-Os analyses were conducted at the Source Rock and Sulfide Geochronology and
620
621
622 206 Geochemistry Laboratory at Durham University. The analytical method is described below.
623
624 207 The purified mineral separate of about 400 mg was accurately weighed and loaded into a
625
626
627 208 Carius tube with a known amount of mixed Re-Os tracer solution containing ^{185}Re and ^{190}Os ,
628
629 209 and a mixture of 11 N HCl (3 ml) and 15.5 N HNO₃ (6 ml) (inverse aqua regia). The Carius
630
631
632 210 tube was sealed and then placed into an oven at 220 °C for 24 h to permit sample and tracer
633
634 211 digestion and equilibration. Osmium was isolated from the inverse aqua regia using solvent
635
636
637 212 extraction (CHCl₃) method and purified by microdistillation, and rhenium was isolated using
638
639 213 solvent extraction (NaOH-acetone) followed by anion column chromatography methods
640
641
642 214 (Selby et al., 2009; Cumming et al., 2013). The purified Re and Os were loaded onto
643
644 215 outgassed Ni and Pt filaments with corresponding activators (barium nitrate and sodium-

650
651
652
653 216 barium hydroxide), respectively (Selby et al., 2009). The Re and Os isotope compositions
654
655
656 217 were measured using negative thermal ionization mass spectrometry on a Thermo Scientific
657
658 218 TRITON mass spectrometer using static Faraday collection for Re and secondary electron
659
660
661 219 multiplier in peak-hopping mode for Os. Total procedural blanks of this study for Re and Os
662
663 220 were 2.3 +/- 0.2 and 0.08 +/- 0.02 pg, with an average $^{187}\text{Os}/^{188}\text{Os}$ value of 0.25 ± 0.05 (n =
664
665
666 221 3). All uncertainties are calculated by error propagation of uncertainties in Re and Os mass
667
668 222 spectrometer measurements, blank abundances and isotopic compositions, spike calibrations,
669
670
671 223 sample and spike weights, and reproducibility of standard Re and Os isotope values. The
672
673 224 operational conditions of the mass spectrometer were monitored by solution reference
674
675
676 225 materials which yielded values of 0.16087 ± 0.00026 for DROsS and 0.5993 ± 0.0006 (1SD,
677
678 226 n=9) for the Re standard. These values are in agreement with those reported previously (e.g.,
679
680
681 227 Selby, 2007; Nowell et al., 2008). The Re-Os isochron age, ^{187}Re - $^{187}\text{Os}^r$ isochron age, and
682
683 228 weighted mean age were determined using Isoplot/Ex_version 3.75 (Ludwig, 2012).

685 229 **4. Results**

687
688 230 The Re-Os data are presented in Table 1 and Figures 7 – 10. The Re and Os abundances in
689
690
691 231 the pyrite from the stage II vein in the Guoluolongwa gold deposit varies widely, from 0.06
692
693 232 to 0.57 ppb and 1.5 to 228.8 ppt, respectively. The $^{187}\text{Re}/^{188}\text{Os}$ (4.57 – 4917.48) and
694
695
696 233 $^{187}\text{Os}/^{188}\text{Os}$ (0.15 – 31.19) ratios display highly variable values and yield a Re-Os isochron
697
698 234 Model 3 date of 374 ± 15 Ma (MSWD = 4.6) and initial $^{187}\text{Os}/^{188}\text{Os}$ (Osi) of 0.06 ± 0.22 .
699
700
701 235 Using the Osi value from the isochron, with the exception of Au4-1, the sample set possesses
702
703 236 ≥ 93 % radiogenic ^{187}Os ($^{187}\text{Os}^r$) and are therefore characterized as low level highly
704
705
706
707
708

709
710
711
712 237 radiogenic sulfides (LLHR, [Stein et al., 2000](#)). In contrast, sample Au4-1 exhibits a high
713
714 238 abundance of common Os ($^{192}\text{Os} = 94.2$ ppt). Individually, the six LLHR samples yield Re-
715
716
717 239 Os model dates of 353 – 394 Ma (Table 1 and [Fig. 7C](#)), with a weighted mean age of $375 \pm$
718
719
720 240 11 Ma (MSWD = 0.60; [Fig. 7C](#)) and ^{187}Re - $^{187}\text{Os}^r$ isochron date of 373 ± 17 Ma ([Fig. 7B](#);
721
722 241 MSWD = 0.68; initial $^{187}\text{Os}^r = 0.01 \pm 0.05$). For the sample Au4-1, calculation of model age
723
724 242 using the Osi from the isochron yields a highly imprecise and inaccurate date (1147 ± 5724
725
726
727 243 Ma; Table 1). Further, the weighted average (375 ± 11 Ma; MSWD = 0.51) and ^{187}Re - $^{187}\text{Os}^r$
728
729
730 244 isochron date (373 ± 17 Ma; MSWD = 0.56; initial $^{187}\text{Os}^r = 0.01 \pm 0.06$) is not appreciably
731
732 245 affected including data of the sample Au4-1.

733
734 246 Using a date of 375 Ma, the six LLHR samples yield either positive or negative Osi values
735
736
737 247 with significant uncertainties (Table 1), with the non-radiogenic sample, Au4-1, yielding an
738
739
740 248 Osi value of 0.12 ± 0.01 (Table 1 and [Fig. 10](#)). Based on this Osi value, model dates for all
741
742 249 samples are recalculated, which yield a weighted mean date of 365 ± 16 Ma (all samples;
743
744
745 250 MSWD = 3.70; [Fig. 7C](#)) and 365 ± 19 Ma (excluding sample Au4-1; MSWD = 4.4; [Fig. 7C](#)).

746
747 251 The Re and Os abundances in pyrite from the stage III vein of the Guoluolongwa gold
748
749
750 252 deposit are 0.17 – 0.62 ppb and 1.4 – 3.7 ppt, respectively. The chalcopyrite mineral
751
752 253 separates display much lower Re abundances (0.01 – 0.06 ppb) and wide range of Os contents
753
754
755 254 ($0.8 - 322.2$ ppt). As a whole, the $^{187}\text{Re}/^{188}\text{Os}$ (0.24 – 2809.52) and $^{187}\text{Os}/^{188}\text{Os}$ (0.13 – 16.91)
756
757 255 data from the four pyrites and the three chalcopyrites yield a Model 1 Re-Os isochron date of
758
759
760 256 354 ± 7 Ma (MSWD = 0.18; [Fig. 8A](#)), with non-radiogenic Osi value of 0.13 ± 0.01 . Based
761
762 257 on the Osi value defined by the Re-Os isochron, five samples possess $> 93\%$ $^{187}\text{Os}^r$ and two
763
764
765
766
767

768
769
770
771 258 samples show a high abundance of common Os ($^{192}\text{Os} = 16.5$ and 132.9 ppt). Individually,
772
773 259 the LLHR samples yield Re-Os model dates between 349 and 407 Ma, with the two non-
774
775
776 260 radiogenic samples possessing large uncertainties (Table 1 and Fig. 8C). The ^{187}Re - $^{187}\text{Os}^f$
777
778
779 261 isochron date based on the five LLHR samples (355 ± 11 Ma; MSWD = 0.16; initial $^{187}\text{Os}^f =$
780
781 262 0.00 ± 0.02 ; Fig. 7B) and all samples (355 ± 11 Ma; MSWD = 0.10; initial $^{187}\text{Os}^f = 0.00 \pm$
782
783 263 0.01 ; Fig. 7B), are identical and so are the weighted mean dates (354 ± 7 Ma; Fig. 7C). The
784
785
786 264 Osi values of individual samples calculated based on the weighted mean date vary from 0.05
787
788
789 265 to 0.32, with the LLHR samples showing significant uncertainties. (Table 1 and Fig. 10)

791 266 The Re and Os abundances of pyrite from the Stage II quartz vein of the Annage gold
792
793
794 267 deposit range from 2.4 to 7.6 ppb and 21.9 to 105.1 ppt, respectively (Table 1). The
795
796 268 $^{187}\text{Re}/^{188}\text{Os}$ (299.13 – 28139.20) and $^{187}\text{Os}/^{188}\text{Os}$ (5.53 – 145.66) ratios vary greatly and yield
797
798
799 269 a Re-Os isochron date of 369 ± 18 Ma (MSWD = 24), with radiogenic Osi value of 3.9 ± 2.4
800
801 270 (Fig. 9A). Discarding the sample CK003 that deviates the isochron, the remaining nine
802
803
804 271 samples yield an isochron date of 382.6 ± 8.0 Ma, with a much more precise Osi value (3.65
805
806 272 ± 0.51) and smaller MSWD (6.6; Fig. 9B), indicating that sample CK003 is the cause of the
807
808
809 273 scatter in the linear regression analysis. Using the Osi value of 3.65 ± 0.51 , the Re-Os model
810
811 274 dates of the nine samples range from 370 to 460 Ma (Table 1 and Fig. 9D). A ^{187}Re - $^{187}\text{Os}^f$
812
813
814 275 isochron date of 396 ± 28 Ma (initial $^{187}\text{Os}^f = -0.8 \pm 1.5$; MSWD = 0.42) and a weighted mean
815
816 276 age of 383 ± 6 Ma (MSWD = 0.57) is determined based on the nine samples. Further, using
817
818
819 277 the Osi value of 3.65 ± 0.51 , the outlier sample, CK003, yields a model age of 349 ± 6 Ma
820
821 278 that approach the isochron age of stage III veins of the Guoluolongwa gold deposit (Table 1).
822
823
824
825
826

827
828
829
830 **279 5. Discussion**
831

832
833 **280 5.1 Evaluation of the Re-Os dates and Osi values**
834

835
836 **281** The Re-Os isochron date (Fig. 7A; 375 ± 15 Ma) and the ^{187}Re - $^{187}\text{Os}^r$ isochron date (Fig. 7B;
837
838 **282** 373 ± 17 Ma) determined from the stage II veins in the Guoluolongwa gold deposit are
839
840
841 **283** identical including uncertainty. The weighted mean of the Re-Os model dates based on the
842
843 **284** Osi value from the Re-Os isochron (0.06 ± 0.22) is in agreement with the age based on the
844
845 **285** Osi value calculated for the non-radiogenic sample Au4-1 (0.12 ± 0.01) within uncertainty.
846
847
848 **286** However, the Re-Os model dates determined based on an Osi value of 0.12 ± 0.01 are
849
850
851 **287** nominally younger than the date obtained from that based on Osi value of 0.06 ± 0.22 (365
852
853 **288** vs. 375 Ma; Fig. 7) and show much higher MSWD (3.7 and 4.4 vs. 0.5 and 0.6; Fig. 7C). The
854
855
856 **289** reason for this is the greater precision in the model Re-Os dates determined using an Osi
857
858 **290** value of 0.06 ± 0.22 relative to 0.12 ± 0.01 . Regardless, all Re-Os date determinations
859
860
861 **291** indicate that stage II mineralization at the Guoluolongwa occurred at ~ 370 Ma suggesting the
862
863 **292** interval of mineralization occurred between the Latest Devonian and Earliest Carboniferous.

864
865
866 **293** The Osi value from the Re-Os isochron and the LLHR samples show significant
867
868 **294** uncertainties (Fig. 7A and Table 1), making the geological significance of these Osi values
869
870
871 **295** ambiguous. However, the Re-Os data for the non-radiogenic sample (Au4-1) yields a highly
872
873 **296** precise Osi value (0.12 ± 0.01). Considering the much higher common Os of this sample
874
875
876 **297** (Au4-1) than those for the LLHR samples, the ^{188}Os determination of this sample is more
877
878 **298** reliable and so is the Osi value (Stein et al., 2000). Consequently, we take 0.12 ± 0.01 to
879
880
881
882
883
884
885

886
887
888
889 299 represent the best estimate of Osi composition of these samples, which is almost identical to
890
891 300 Osi values of the stage III vein in the Guoluolongwa gold deposit (discussed below).
892

893
894 301 The Re-Os isochron date (354 ± 7 Ma), ^{187}Re - $^{187}\text{Os}_r$ isochron date (355 ± 11 Ma) and
895
896 302 weighted mean dates (354 ± 7 Ma) based on all samples from the stage III vein in the
897
898 303 Guoluolongwa gold deposit are identical, with the MSWD values corresponding to these
899
900 304 dates being < 0.3 , indicating that the degree of scattering in the data set is almost entirely
901
902 305 analytical. As such the timing of the stage III mineralization is taken to be ~ 355 Ma ($\pm 7 - 11$).
903
904 306 The Osi values from the Re-Os isochron and the non-radiogenic samples are consistent, at
905
906 307 0.13 ± 0.01 , which are taken to represent the best estimate of the Osi composition of the stage
907
908 308 III mineralization.
909

910
911
912 309 The two Re-Os isochron dates (369 ± 18 Ma (all samples) and 383 ± 8 Ma (excluding
913
914 310 sample CK003)) from the stage II quartz veins in the Annage gold deposit are similar
915
916 311 including the uncertainty. However, the uncertainty of the age 369 Ma is much larger (18 vs.
917
918 312 8 Ma) and so is the uncertainty in the corresponding Osi (2.4 vs. 0.5) and degree of scatter
919
920 313 about the best fit of the data (MSWD = 24 vs. 6.6). The scatter coupled with the obvious
921
922 314 deviation of the CK003 from the best fit of all the Re-Os data (Fig. 9A) indicate the CK003
923
924 315 could relate to a different stage of mineralization from that of the stage III mineralization
925
926 316 and/or its Re-Os systematics are slightly disturbed. The model Re-Os date for sample CK003
927
928 317 is much younger than those of other samples (349 ± 6 Ma). As such, we regard the Re-Os
929
930 318 isochron date determined from all samples with the exception of CK003 (383 ± 8 Ma) as the
931
932 319 best estimate of the timing of the stage II veins at Annage. This age is consistent with the
933
934
935
936
937
938
939
940
941
942
943
944

945
946
947
948 320 weighted mean date of the Re-Os model dates (383 ± 6 Ma) and within the uncertainty of the
949
950 321 ^{187}Re - ^{187}Os isochron date (396 ± 28 Ma). Interestingly, the Re-Os model date of the sample
952
953 322 CK003 (349 ± 6 Ma) is consistent with that of stage III veins in the Guoluolongwa gold
954
955 323 deposit, indicating that a common Carboniferous event may occur in the two deposit. The Osi
957
958 324 value from the Re-Os isochron (3.65 ± 0.51) is similar to those calculated for each sample
959
960 325 (~ 2.9 to 4.3 excluding CK003) and could be taken to represent the initial compositions of
962
963 326 these samples.

965 327 *5.2 Multiple gold-mineralizing events in the East Kunlun Orogen*

968 328 Muscovite collected from the gold-bearing vein in the Guoluolongwa yields a Late Triassic
969
970 329 $^{40}\text{Ar}/^{39}\text{Ar}$ plateau age that was interpreted as the timing of gold mineralization (202.7 ± 1.5
972
973 330 Ma; [Xiao et al., 2014](#)). Although, no detailed paragenesis between the muscovite and
974
975 331 gold/gold-bearing minerals are reported ([Xiao et al., 2014](#)), it is considered that the
976
977 332 Guoluolongwa gold deposit, and even all gold deposits in the Gouli goldfield, are Triassic in
978
979 333 age, similar to many other gold deposits/fields in the East Kunlun Orogen and adjacent areas,
982
983 334 e.g., Wulonggou (sericite Ar-Ar, 236.5 ± 0.5 Ma; [Zhang et al., 2005](#)), Shuizhadonggou
984
985 335 (deposit in the Wulonggou gold field; sericite Ar-Ar, 237-231 Ma; [Zhang et al., 2017](#)) and
987
988 336 Dachang (sericite Ar-Ar, 218.6 ± 3.2 Ma; [Zhang et al., 2005](#)). However, the Re-Os data
989
990 337 obtained from directly analyzing of sulfides (pyrite and chalcopyrite) from the Guoluolongwa
992
993 338 and Annage yield much older ages (Late Devonian and Early Carboniferous) and thus it is
994
995 339 necessary to re-evaluate the Triassic age gained from Ar-Ar dating and timing of gold
997
998 340 mineralization of these deposits in the East Kunlun Orogen.

1004
1005
1006
1007 341 Crosscutting relationships of different geological units can offer the first-order constraint
1008
1009 342 on the timing of the gold mineralizing events. In the Guoluolongwa gold deposit, field
1010
1011
1012 343 observations indicate that the hydrothermal veins related to gold mineralization cut cross the
1013
1014 344 gabbro (416.2 ± 3.5 Ma; [Yue et al., 2013](#)) and the stage II pyrite-quartz vein are crosscut by
1015
1016
1017 345 the stage III polymetallic sulfides-quartz veins ([Fig.5 A](#)). Thus, both types of gold-bearing
1018
1019 346 veins should be emplaced after ~ 416 Ma and the stage II pyrite-quartz vein must be older
1020
1021
1022 347 than the stage III polymetallic sulfides-quartz vein. These conclusions are consistent with our
1023
1024
1025 348 data (375 ± 11 Ma and 354 ± 7 Ma, respectively), but cannot explain the contradictory results
1026
1027 349 between our Re-Os dates and the previously reported muscovite Ar-Ar age (202.7 ± 1.5 Ma;
1028
1029
1030 350 [Xiao et al., 2014](#)). Two possible models are: (1) the Paleozoic ages obtained from the Re-Os
1031
1032 351 data of the sulfides represent the timing of gold mineralization, with the $^{40}\text{Ar}/^{39}\text{Ar}$ plateau age
1033
1034 352 from muscovite being a product of a late thermal/hydrothermal overprint; (2) the $^{40}\text{Ar}/^{39}\text{Ar}$
1035
1036 353 plateau age represent the timing of gold mineralization, while sulfides were contaminated by
1037
1038
1039 354 old rocks during fluid migration leading to inhomogeneous initial $^{187}\text{Os}/^{188}\text{Os}$ compositions
1040
1041
1042 355 of sulfide samples and thus result in an errorchron or pseudochron ([Yang et al., 2008](#)). A
1043
1044
1045 356 valid method to test the two models is to plot initial $^{187}\text{Os}/^{188}\text{Os}$ against $1/^{192}\text{Os}$ ([Faure and](#)
1046
1047 357 [Mensing, 2005](#)). If model two is correct, a linear relationship between the initial $^{187}\text{Os}/^{188}\text{Os}$
1048
1049
1050 358 and $1/^{192}\text{Os}$ should be expressed by the data. However, our data from both the two stages of
1051
1052 359 mineralization (stage II and III) are randomly distributed in $^{187}\text{Os}/^{188}\text{Os}$ vs. $1/^{192}\text{Os}$ space
1053
1054
1055 360 ([Figs. 11a and b](#)), which means the isochrons we obtain represent the best estimate of the
1056
1057 361 timing of gold mineralization, thus indicating Devonian and Carboniferous gold
1058
1059
1060
1061
1062

1063
1064
1065
1066 362 mineralization. In addition, samples from the stage II vein in the Annage gold deposit yield a
1067
1068 363 Devonian age of 383 ± 8 Ma, which is consistent with the age of the stage II vein of the
1069
1070
1071 364 Guoluolongwa gold deposit within uncertainty. The random distribution of the data in
1072
1073
1074 365 $^{187}\text{Os}/^{188}\text{Os}$ vs. $1/^{192}\text{Os}$ space (Fig. 11C) indicate the isochron of the Annage gold deposits
1075
1076 366 should also not be an errorchron or pseudochron (Faure and Mensing, 2005; Yang et al., 2008)
1077
1078 367 and thus the isochron age should represent the formation age of the stage II vein of this
1079
1080
1081 368 deposit, which support the Devonian gold mineralizing event occurred in the Gouli area. The
1082
1083
1084 369 Re-Os model date of the sample CK003 (349 ± 6 Ma) from the Annage gold deposit, is
1085
1086 370 identical with the Carboniferous age of stage III veins in the Guoluolongwa gold deposit,
1087
1088
1089 371 which further implies that this gold mineralizing event occurred in the Gouli gold field during
1090
1091 372 the Early Carboniferous. Furthermore, the contemporaneous Devonian gold-mineralizing
1092
1093
1094 373 event has been revealed to the north of the East Kunlun Orogen (Qilian-Qaidam; Sericite Ar-
1095
1096 374 Ar, 409-372 Ma; Yang et al., 2005; Zhang et al., 2005), indicating the existence of a
1097
1098
1099 375 Devonian gold-mineralizing event regionally. Consequently, we interpret the two episodes
1100
1101 376 recorded by our Re-Os data from both the Guoluolongwa and Annage gold deposits as the
1102
1103
1104 377 formation ages of stage II and III veins in the Gouli gold field, respectively. In this context,
1105
1106 378 the early reported muscovite Ar-Ar age is considered to represent a later
1107
1108
1109 379 thermal/hydrothermal activity that may be related to the pervasive Permian-Triassic
1110
1111 380 magmatic event in the East Kunlun Orogen (Chen et al., 2017). Whether this later
1112
1113
1114 381 thermal/hydrothermal activity contribute gold to the two deposits deserve further study.
1115
1116 382 Based on the present evidence, we prefer that the later thermal/hydrothermal activity
1117
1118
1119
1120
1121

1122
1123
1124
1125 383 (Triassic) is unlikely to contribute significant gold to the two deposits, since a later gold-
1126
1127
1128 384 bearing fluid should affect the Re-Os system of the dating mineral formed early or form new
1129
1130 385 dating mineral (such as gold-bearing pyrite) which is closely relate to gold in the studied area.
1131
1132
1133 386 Our Re-Os data do not record any information of this Triassic event and no new gold-bearing
1134
1135 387 assemblage or vein has been found by field observation.
1136

1137
1138 388 From a regional perspective, with the exception of the Guoluolongwa and Annage gold
1139
1140 389 deposits that occur in Proterozoic or Ordovician-Silurian metamorphic rocks, the three other
1141
1142
1143 390 gold deposits in the Gouli goldfield crosscut Triassic (Asiha and Delong) or Silurian
1144
1145 391 (Walega) aged intrusions (Fig. 2) and show distinct mineralization styles from those of
1146
1147
1148 392 Guoluolongwa and Annage (Li et al., 2012; Chen, 2018), indicating different gold-
1149
1150 393 mineralizing events forming these deposits. Thus at least one Triassic or post-Triassic gold-
1151
1152
1153 394 mineralizing event occurred in the Gouli goldfield based on the cross-cutting relationship
1154
1155 395 between orebodies and Triassic intrusion (Li et al., 2014), which is likely to be the same
1156
1157
1158 396 Triassic event leading to the formation of the Wulonggou goldfield to the west of the Gouli
1159
1160 397 (Zhang et al., 2017). Consequently, together with the Late Paleozoic (Devonian and
1161
1162
1163 398 Carboniferous) mineralization revealed by our Re-Os data, there are at least two gold-
1164
1165 399 mineralizing epochs (Late Paleozoic and Late Triassic) in the Gouli goldfield.
1166

1167 400 *5.3 Source of ore-forming materials and implications on the genetic model*

1168
1169
1170 401 The geochronological data presented above improve the framework of the temporal
1171
1172
1173 402 relationships between gold mineralization and tectonic-magmatic activities (discussed below)
1174
1175 403 that may directly contribute to the formation of the gold deposits. However, timing constraint
1176
1177
1178
1179
1180

1181
1182
1183
1184
1185
1186
1187
1188
1189
1190
1191
1192
1193
1194
1195
1196
1197
1198
1199
1200
1201
1202
1203
1204
1205
1206
1207
1208
1209
1210
1211
1212
1213
1214
1215
1216
1217
1218
1219
1220
1221
1222
1223
1224
1225
1226
1227
1228
1229
1230
1231
1232
1233
1234
1235
1236
1237
1238
1239

404 alone does not distinguish between rock types or reservoirs that may have contributed to the
405 formation of these gold deposits. In this regard, the Osi values of the sulfides from the Gouli
406 goldfield can provide a unique insight into the ore-forming process (e.g., [Morelli et al., 2007](#);
407 [Morelli et al., 2010](#)).

408 As discussed above, the non-radiogenic Osi values of the stage II (0.12 ± 0.01) and III
409 (0.13 ± 0.1) veins in the Guoluolongwa gold deposit are consistent, similar to that of the
410 mantle ([Fig. 10](#); $\sim 0.12\text{--}0.13$; [Shirey and Walker, 1998](#)), indicating mantle or extremely
411 juvenile crustal source of Os, by inference the ore metal (Au). This also excludes the wall
412 rocks of the Naij Tal Group or possibly the concealed Proterozoic metamorphic basement
413 rocks as the sources of the ore-forming materials ([Fig. 10](#)). Considering the contemporaneous
414 mantle-derived mafic rocks in the East Kunlun Orogen (345 – 380 Ma; [Chen et al., 2001](#); [Bao
415 et al., 2013](#)), we contend that the ore metals of the two vein types of the Guoluolongwa gold
416 deposit were derived from partial melting of the mantle. As to the ore-forming fluids,
417 previously reported H-O isotopes (e.g., [Wang, 2012](#); [Yue, 2013](#); [Xiao et al., 2014](#)) indicate
418 they were derived mainly from magmatic sources ([Fig. 12](#)) ([Chen, 2018](#)). The $\delta^{34}\text{S}$ of the
419 Guoluolongwa gold deposit shows a range of $-6\text{‰} - 5.2\text{‰}$ ([Chen, 2018](#) and references
420 therein), a much wider range than that of mantle-derived sulfur ($\delta^{34}\text{S}=0\pm 3\text{‰}$), indicating
421 crustal sulfur may also contribute to the mineralization. Taken together, the origin of the
422 Guoluolongwa gold deposit is different to that of typical orogenic gold deposits whose ore
423 metal and fluids are considered to be derived from old metamorphic rocks ([Goldfarb et al.,
424 2005](#) and references therein). It is also noteworthy that there is a nominally ~ 20 Ma age gap

1240
1241
1242
1243
1244
1245
1246
1247
1248
1249
1250
1251
1252
1253
1254
1255
1256
1257
1258
1259
1260
1261
1262
1263
1264
1265
1266
1267
1268
1269
1270
1271
1272
1273
1274
1275
1276
1277
1278
1279
1280
1281
1282
1283
1284
1285
1286
1287
1288
1289
1290
1291
1292
1293
1294
1295
1296
1297
1298

425 between the formations of the two gold-bearing vein types. Such a large age gap is likely to
426 imply two separately magmatic events contributing to the formation of the two vein types
427 instead of a continuous hydrothermal activity, which could also explain the different mineral
428 assemblages between the two vein types. In summary, the Guoluolongwa gold deposit is
429 considered to be of magmatic origin and formed in relation to multiple magmatic events.

430 For the Annage gold deposit, considering the close spatial relationship (<3km),
431 contemporaneous mineralization (Figs. 7 – 10), identical mineralization styles and mineral
432 assemblages (Figs. 5 – 6), and consistent H-O isotope compositions (Fig. 12) between the
433 Guoluolongwa and Annage deposits, we contend that the two deposits should have similar
434 origin, which suggests that mantle-derived fluids and metals contributed to the formation of
435 the Annage deposit. However, the Osi values of the sulfides from this deposit are much
436 higher than that of the mantle (~0.12 – 0.13; Shirey and Walker, 1998), indicating another
437 radiogenic source supplied the Os of this deposit. Considering the specific geological
438 background of the two deposits, wall rocks, i.e. the Ordovician-Silurian (Naij Tal Group) and
439 Proterozoic metamorphic rocks (Figs. 3 and 4), are likely candidates leading to the high Osi
440 values of the stage II gold-bearing veins. The protoliths of the Ordovician-Silurian
441 metamorphic rocks are mudstone and volcanic rocks that were formed in the marine
442 environment (Chen et al., 2013; Chen et al., 2014). Thus, the mudstone should have a similar
443 initial $^{187}\text{Os}/^{188}\text{Os}$ ratio with that of the Ordovician-Silurian sea water (0.28-1.08; 449 Ma;
444 Finlay et al., 2010). Considering ~70 Ma (time gap between 449 Ma and 383 Ma) of ^{187}Os
445 ingrowth from ^{187}Re decay, the $^{187}\text{Os}/^{188}\text{Os}$ ratio of the Ordovician-Silurian black shale (0.6

1299
1300
1301
1302 446 to 1.9; Fig. 10) is much lower than the Osi value of the stage II veins, indicating that the
1303
1304 447 mudstone is likely not be the sole source of the Os in the stage II veins. Further, the volcanic
1305
1306
1307 448 rocks of the Naj Tal Group that formed at 429 Ma had a similar initial $^{187}\text{Os}/^{188}\text{Os}$ (429 Ma)
1308
1309 449 ratio with that of the mantle (Feng et al., 2009). Taking into account of the mantle-like initial
1310
1311
1312 450 $^{187}\text{Os}/^{188}\text{Os}$ ratios and Os accumulation due to ^{187}Re decay, our calculation indicates that the
1313
1314 451 volcanic rocks must have $^{187}\text{Re}/^{188}\text{Os} > 4600$ to gain high $^{187}\text{Os}/^{188}\text{Os}$ ratio of 3.65 at 383 Ma,
1315
1316
1317 452 which is unlikely to be true (Shirey and Walker, 1998). Taken together, the Ordovician-
1318
1319
1320 453 Silurian metamorphic rocks (the host rocks of the Guoluolongwa gold deposit) are unlikely to
1321
1322 454 be the main Os source of the stage II vein in the Annage gold deposit, which is consistent
1323
1324
1325 455 with the low initial $^{187}\text{Os}/^{188}\text{Os}$ ratios of the Guoluolongwa gold deposit. The reported age for
1326
1327 456 the Proterozoic metamorphic rocks in the Gouli area is 904 Ma that represents the age of the
1328
1329
1330 457 protoliths (Fig. 2; Chen et al., 2006). If these rocks are the source of the Os, the Proterozoic
1331
1332 458 metamorphic rocks would have $^{187}\text{Re}/^{188}\text{Os}$ values between 300 and 500 to produce the
1333
1334
1335 459 observed Osi of the sulfides (Fig. 10). Geological units that have such high $^{187}\text{Re}/^{188}\text{Os}$ could
1336
1337 460 be basalts or black shales (Shirey and Walker, 1998) that are possible protoliths of the
1338
1339
1340 461 Proterozoic metamorphic rocks given these rocks contain amphibolite and schist (Fig. 4).
1341
1342 462 Thus, it is likely that the Proterozoic metamorphic rocks are the main source of the Os
1343
1344
1345 463 associated with stage II veins, which is supported by that the host rocks of orebody I, where
1346
1347 464 the samples collected, are Proterozoic metamorphic rocks (Fig. 4). Consequently, in addition
1348
1349
1350 465 to the same mineralizing process in the Guoluolongwa gold deposit, the ore-forming fluids of
1351
1352 466 the Annage gold deposit likely reacted with the Proterozoic metamorphic wall rocks that
1353
1354
1355
1356
1357

1358
1359
1360
1361 467 released leached radiogenic Os to the fluids and changed the initial non-radiogenic Os
1362
1363 468 compositions (0.12 – 0.13) to a radiogenic composition (3.65). However, whether this
1364
1365
1366 469 process added crustal ore metal (Os and Au) to the Annage gold deposit need further study.
1367

1368
1369 470 *5.4 Relationships between gold mineralization and tectonic-magmatic activities and*
1370
1371 471 *significance on regional exploration*
1372

1373 472 Regionally, two gold-mineralizing epochs are revealed from our Re-Os data (Late Devonian
1374
1375
1376 473 and Early Carboniferous), published Ar-Ar dating and field observations (Triassic; e.g.,
1377
1378
1379 474 [Zhang et al., 2017](#)). Interestingly, all the gold mineralizing events overlap with emplacement
1380
1381 475 of A-type granites and mafic rocks ([Fig. 13](#)), which indicate the extensional regime within the
1382
1383
1384 476 East Kunlun Orogen. Considering the geological background of the East Kunlun Orogen
1385
1386 477 ([Chen et al., 2017](#)), the two gold-mineralizing epochs should occur during the post-collisional
1387
1388
1389 478 stages related to the evolution of the Prototethys Ocean and Paleotethys Ocean, respectively
1390
1391 479 ([Fig. 13](#)), with the ore-forming fluids being derived from a juvenile magma ([Fig. 12](#)). In this
1392
1393
1394 480 context, gold mineralization in the East Kunlun Orogen should be genetically related to post-
1395
1396 481 collisional magmatism that supplied auriferous fluids.
1397

1398
1399 482 From a more regional perspective, a number of gold deposits have been reported in the
1400
1401 483 adjacent western Qinling (to the immediate west of the East Kunlun Orogen; [Figs. 1A and B](#))
1402
1403
1404 484 ([Liu et al., 2015](#)) and Qilian-Qaidam (to the north of the East Kunlun Orogen; [Figs. 1 A and](#)
1405
1406 485 [B](#)) ([Zhang et al., 2005](#)). In these areas, both lode and disseminated gold deposits are present
1407
1408
1409 486 and most of these gold deposits are hosted in Proterozoic – Early Paleozoic (Qilian-Qaidam)
1410
1411 487 ([Zhang et al., 2005](#)) and Devonian (western Qinling) ([Liu et al., 2015](#)) (metamorphic)
1412
1413
1414
1415
1416

1417
1418
1419
1420 488 volcanic-sedimentary rocks, similar to those of gold deposits in the East Kunlun Orogen.
1421
1422 489 Many of these gold deposits exhibit similar H-O isotopes with those in the East Kunlun
1423
1424
1425 490 Orogen (Fig. 12), indicating magmatic fluids with minor meteoric water played an important
1426
1427
1428 491 role in the mineralizing process (e.g., Fan et al., 2008; Liu et al., 2015; Zhang et al., 2017). In
1429
1430 492 addition, the currently reported ages of these gold deposits display two peaks (Late Paleozoic
1431
1432 493 and Triassic) of gold mineralization (Fig. 13). These ages, integrated with the geological
1433
1434
1435 494 background, indicate that most of these gold deposits were formed in collisional or post-
1436
1437
1438 495 collisional regime related to the evolution of the Prototethys Ocean and Paleotethys Ocean
1439
1440 496 (Fig. 13). In summary, it is likely that common tectonic-magmatic activities controlled the
1441
1442
1443 497 formation of gold deposits from the East Kunlun Orogen, Qilian-Qaidam and western
1444
1445 498 Qinling, all of which are located in the west of the Central Orogenic Belt (Fig. 1A) that are
1446
1447
1448 499 controlled by the evolution of the Prototethys Ocean and Paleotethys Ocean (Qiu and
1449
1450 500 Wijbrans, 2008; Wu and Zheng, 2013). Thus, considering the common geological
1451
1452
1453 501 background and the gold ore-forming potential of the whole western Central Orogenic Belt, it
1454
1455 502 is possible that more Late Paleozoic gold deposits may be revealed in these areas, especially
1456
1457
1458 503 in the western Qinling where multiple magmatic activities developed, but only indirect dating
1459
1460 504 methods (e.g., Ar-Ar dating of micaceous minerals) have been applied (Fig. 13 and related
1461
1462
1463 505 references).

1465 506 **7. Conclusions**

1466
1467
1468 507 Pyrites and chalcopyrites from gold-bearing ores in the Guoluolongwa gold deposit in the
1469
1470 508 Gouli goldfield yield Re-Os ages of 375 ± 11 Ma for the stage II pyrite-quartz vein and $354 \pm$
1471
1472
1473
1474
1475

1476
1477
1478
1479 509 7 Ma for the stage III polymetallic sulfides-quartz vein, which are also recorded by the stage
1480
1481
1482 510 II pyrites from the adjacent Annage gold deposit (383 ± 6 Ma and 349 ± 6 Ma). These data,
1483
1484 511 together with field observations indicate that at least three gold mineralizing events (two in
1485
1486
1487 512 Late Paleozoic and one in Late Triassic) occurred in the Gouli goldfield. The Os values of
1488
1489 513 sulfides indicate that Os and by inference, the ore metal (Au) of the Guoluolongwa deposits
1490
1491
1492 514 were derived from mantle-derived magma. A common ore metal source is also recommended
1493
1494 515 for the Annage gold deposit, but the Os of this deposit is considered to be derived from both
1495
1496
1497 516 the mantle and Proterozoic wall rocks. Results from this study together with previously
1498
1499 517 reported ages of gold mineralization in the East Kunlun Orogen and adjacent areas, indicate
1500
1501
1502 518 that there are two gold-mineralizing epochs (Late Paleozoic and Late Triassic) in the west of
1503
1504 519 the Central Orogenic Belt (included western Qinling, East Kunlun Orogen and Qaidam-
1505
1506
1507 520 Qilian) and all gold mineralizing events occurred in collisional or post-collisional setting
1508
1509 521 related to Tethyan evolution that controlled the whole Central Orogenic Belt. Thus, we infer
1510
1511
1512 522 that more Late Paleozoic gold deposits may be present in the west of Central Orogenic Belt.

1513 1514 523 **8. Acknowledgments**

1515
1516 524 This research was jointly supported by the Fundamental Research Funds for the Central
1517
1518
1519 525 Universities (CUGL17043), the Funds from the East China University of Technology
1520
1521
1522 526 (DHBK2018009 and GJJ180387), and the China Geological Survey (12120114081401,
1523
1524 527 12120114000701). DS acknowledges the Total Endowment Fund. We appreciate fieldwork
1525
1526
1527 528 assistance of Shaoqing Zhao, Zhen Wang, Xiaolong Wang, Yang Tang, Junlin Chen, Yujing
1528
1529 529 Zhao, and Yan Liu from the China University of Geosciences.
1530
1531
1532
1533
1534

1535
1536
1537
1538
1539
1540
1541
1542
1543
1544
1545
1546
1547
1548
1549
1550
1551
1552
1553
1554
1555
1556
1557
1558
1559
1560
1561
1562
1563
1564
1565
1566
1567
1568
1569
1570
1571
1572
1573
1574
1575
1576
1577
1578
1579
1580
1581
1582
1583
1584
1585
1586
1587
1588
1589
1590
1591
1592
1593

530 **References**

531

532 Bao, G.P., Wang, G.L., Liu, R., Han, H.C., 2013, Kayakedengtage area two basic dike rocks

533 geochemistry and significance: *Northwestern Geology*, v. 46, p. 37-43 (in Chinese with

534 English abs.).

535 Bian, Q.T., Li, D.H., Pospelov, I., Yin, L.M., Li, H.S., Zhao, D.S., Chang, C.F., Luo, X.Q.,

536 Gao, S.L., Astrakhantsev, O., Chamov, N., 2004, Age, geochemistry and tectonic setting

537 of Buqingshan ophiolites, North Qinghai-Tibet Plateau, China: *Journal of Asian Earth*

538 *Sciences*, v. 23, p. 577-596.

539 Chen, J., Wei, J., Fu, L., Li, H., Zhou, H., Zhao, X., Zhan, X., Tan, J., 2017, Multiple sources

540 of the Early Mesozoic Gouli batholith, Eastern Kunlun Orogenic Belt, northern Tibetan

541 Plateau: Linking continental crustal growth with oceanic subduction: *Lithos*, v. 292-293,

542 p. 161-178.

543 Chen, L., Sun, Y., Pei, X.Z., Gao, M., Tao, F., Zhang, Z.Q., Chen, W., 2001, Northernmost

544 Paleo-Tethyan oceanic basin in Tibet: geochronological evidence from $^{40}\text{Ar}/^{39}\text{Ar}$ age

545 dating of Dur'ngoi ophiolite: *Chinese Science Bulletin*, v. 46, p. 1203-1205.

546 Chen, X.H., Gehrels, G., An, Y., Li, L., Jiang, R.B., 2012, Paleozoic and Mesozoic basement

547 magmatism of Eastern Qaidam Basin, Northern Qinghai-Tibet Plateau: LA-ICP-MS

548 zircon U-Pb geochronology and its geological significance: *Acta Geologica Sinica*, v. 86,

549 p. 350-369.

550 Chen, G.J., 2014, Metallogenesis of gold deposits in Gouli regional and peripheral area of

551 East Kunlun, Qinghai province: Ph.D. thesis, Changchun, Jilin University, 165p (in

1594
1595
1596
1597 552 Chinese with English abs.).
1598
1599
1600 553 Chen, J., 2018, Paleozoic-Mesozoic tectono-magmatic evolution and gold mineralization in
1601
1602 554 Gouli Area, east end of East Kunlun Orogen: Ph.D. thesis, Wuhan, China University of
1603
1604 555 Geosciences, 224p (in Chinese with English abs.).
1606
1607 556 Chen, J.J., Fu, L.B., Wei, J.H., Tian, N., Xiong, L., Zhao, Y.J., Zhang, Y.J., Qi, Y.Q., 2016,
1608
1609 557 Geochemical characteristics of Late Ordovician granodiorite in Gouli area, Eastern
1610
1611 558 Kunlun Orogenic Belt, Qinghai province: Implications on the evolution of Proto-Tethys
1613
1614 559 Ocean: Earth Science, v. 41, p. 1863-1882 (in Chinese with English abs.).
1616
1617 560 Chen, N.S., Li, X.Y., Wang, X.Y., Chen, Q., Wang, Q.Y., Wan, Y.S., 2006, Zircon SHRIMP
1618
1619 561 U-Pb age of Neoproterozoic metagranite in the North Kunlun unit on the southern margin
1620
1621 562 of the Qaidam block in China: Geological Bulletin of China, v. 25, p. 1311-1314 (in
1622
1623 563 Chinese with English abs.).
1624
1625 564 Chen, Y.X., Pei, X.Z., Li, R.B., Li, Z.C., Pei, L., Chen, G.C., Liu, C.J., Li, X.B., Yang, J.,
1626
1627 565 2013, Zircon U-Pb age, geochemical characteristics and tectonic significance of
1628
1629 566 metavolcanic rocks from Naj Tal Group, east section of East Kunlun: Earth Science
1630
1631 567 Frontier, v. 20, p. 240-254 (in Chinese with English abs.).
1632
1633 568 Chen, Y.X., Pei, X.Z., Li, R.B., Li, Z.C., Pei, L., Liu, C.J., Yang, J., 2014, Geochemical
1634
1635 569 characteristics and tectonic significance of meta-sedimentary rocks from Naj Tal group,
1636
1637 570 eastern section of East Kunlun: Geoscience, v. 28, p. 489-500 (in Chinese with English
1638
1639 571 abs.).
1640
1641 572 Cumming, V.M., Poulton, S.W., Rooney, A.D., Selby, D., 2013, Anoxia in the terrestrial
1642
1643
1644
1645
1646
1647
1648
1649
1650
1651
1652

1653
1654
1655
1656 573 environment during the late Mesoproterozoic: *Geology*, v. 41, p. 583-586.
1657
1658 574 Ding, C.M., 2007, Genesis of Tanjianshan gold deposit: Qinghai Science and Technology, p.
1659
1660 575 32-36 (in Chinese with English abs.).
1661
1662
1663 576 Ding, Q.F., Jin, S.K., Wang, G., Zhang, B.L., 2013, Ore-Forming fluid of the Guoluolongwa
1664
1665 577 gold deposit in Dulan county, Qinghai province: *Journal of Jilin University (Earth*
1666
1667 578 *Science Edition)*, v. 43, p. 415-426 (in Chinese with English abs.).
1668
1669
1670 579 Esser, B.K., Turekian, K.K., 1993, The osmium isotopic composition of the continental crust:
1671
1672 580 *Geochimica Et Cosmochimica Acta*, v. 57, p. 3093-3104.
1673
1674
1675 581 Fan, J.J., Lu, Y.M., Cong, Y.X., Chang, C.J., 2008, Study on 3 gold deposits varied in
1676
1677 582 characteristics at the north slope of the Danghe Nanshan Mountain in the west Qilian
1678
1679 583 Mountains: *Contributions To Geology and Mineral Resources Research*, v. 23, p. 48-53
1680
1681 584 (in Chinese with English abs.).
1682
1683
1684 585 Fan, J.J., Zhang, X.J., Chang, C.J., Zhang, H.Y., Cong, Y.X., Ren, S., 2006, Geochemistry
1685
1686 586 and genesis of the Jijiaogou gold deposit in Subei, Gansu Province, China: *Geology and*
1687
1688 587 *Resources*, v. 15, p. 272-276 (in Chinese with English abs.).
1689
1690
1691 588 Faure, G., Mensing, T.M., 2005, *Isotopes: principles and applications: 3 ed.* Hoboken, New
1692
1693 589 Jersey, John Wiley & Sons, 897p.
1694
1695
1696 590 Feng, C.Y., Qu, W.J., Zhang, D.Q., Dang, X.Y., Du, A.D., Li, D.X., She, H.Q., 2009, Re-Os
1697
1698 591 dating of pyrite from the Tuolugou stratabound Co(Au) deposit, eastern Kunlun Orogenic
1699
1700 592 Belt, northwestern China: *Ore Geology Reviews*, v. 36, p. 213-220.
1701
1702
1703 593 Feng, C.Y., 2002, Multiple orogenic processes and mineralization of orogenic gold deposits
1704
1705
1706
1707
1708
1709
1710
1711

1712
1713
1714
1715 594 in the East Kunlun Orogen, Qinghai province: Ph.D. thesis, Beijing, Chinese Academy of
1716
1717
1718 595 Geological Sciences, 104p (in Chinese with English abs.).
1719
1720 596 Feng, C.Y., Zhang, D.Q., Wang, F.C., Li, D.X., She, H.Q., 2004, Geochemical characteristics
1721
1722 597 of ore-forming fluids from the orogenic An (and Sb) deposits in the eastern Kunlun area,
1723
1724
1725 598 Qinghai province: *Acta Petrologica Sinica*, v. 20, p. 949-960 (in Chinese with English
1726
1727 599 abs.).
1728
1729
1730 600 Feng, J.Y., Pei, X.Z., Yu, S.L., Ding, S.P., Li, R.B., Sun, Y., Zhang, Y.F., Li, Z.C., Chen,
1731
1732
1733 601 Y.X., Zhang, X.F., Chen, G.C., 2010, The discovery of the mafic-ultramafic melange in
1734
1735 602 Kekesha area of Dulan County, East Kunlun region, and its LA-ICP-MS zircon U-Pb age:
1736
1737 603 *Geology in China*, v. 37, p. 28-38 (in Chinese with English abs.).
1738
1739
1740 604 Finlay, A.J., Selby, D., Gr Cke, D.R., 2010, Tracking the Hirnantian glaciation using Os
1741
1742 605 isotopes: *Earth and Planetary Science Letters*, v. 293, p. 339-348.
1743
1744
1745 606 Goldfarb, R.J., Baker, T., Dube, B., Groves, D.I., Hart, C.J., Gosselin, P., 2005, Distribution,
1746
1747 607 character, and genesis of gold deposits in metamorphic terranes: *Economic Geology*
1748
1749 608 100th Anniversary Volume, p. 407-450.
1750
1751
1752 609 He, D.F., Dong, Y.P., Zhang, F.F., Yang, Z., Sun, S.S., Cheng, B., Zhou, B., Liu, X.M., 2016,
1753
1754 610 The 1.0 Ga S-type granite in the East Kunlun Orogen, Northern Tibetan Plateau:
1755
1756 611 Implications for the Meso- to Neoproterozoic tectonic evolution: *Journal of Asian Earth*
1757
1758 612 *Sciences*, v. 130, p. 46-59.
1759
1760
1761
1762 613 Hu, R.G., 2008, Research on geological-Geochemical characteristics and Genesis of the
1763
1764 614 Guoluolongwa gold deposit in Qinghai Province: master thesis, Changsha, Central South
1765
1766
1767
1768
1769
1770

1771
1772
1773
1774 615 University, 99p (in Chinese with English abs.).
1775
1776 616 Kong, H.L., Li, J.C., Li, Y.Z., Jia, Q.Z., Yang, B.R., 2014, Geochemistry and zircon U-Pb
1777
1778
1779 617 geochronology of Annage diorite in the eastern section from East Kunlun in Qinghai
1780
1781
1782 618 province: Geological Science and Technology Information, v. 33, p. 11-17 (in Chinese
1783
1784 619 with English abs.).
1785
1786 620 Lawley, C., Selby, D., Imber, J., 2013, Re-Os molybdenite, pyrite, and chalcopyrite
1787
1788
1789 621 geochronology, Lupa goldfield, southwestern Tanzania: tracing metallogenic time scales
1790
1791
1792 622 at midcrustal shear zones hosting orogenic Au deposits: Economic Geology, v. 108, p.
1793
1794 623 1591-1613.
1795
1796 624 Li, R.B., Pei, X.Z., Li, Z.C., Pei, L., Liu, C.J., Chen, Y.X., Chen, G.C., Liu, Z.Q., Yang, J.,
1797
1798
1799 625 2015, Geochemistry and zircon U-Pb geochronology of granitic rocks in the Buqingshan
1800
1801
1802 626 tectonic mélangé belt, northern Tibet Plateau, China and its implications for Prototethyan
1803
1804 627 evolution: Journal of Asian Earth Sciences, v. 105, p. 374-389.
1805
1806 628 Li, R.B., Pei, X.Z., Li, Z.C., Sun, Y., Feng, J.Y., Lei, P., Chen, G.C., Liu, C.J., Chen, Y.X.,
1807
1808
1809 629 2013, Geochemical features, age, and tectonic significance of the Kekekete mafic-
1810
1811
1812 630 ultramafic rocks, East Kunlun Orogen, China: Acta Geologica Sinica, v. 87, p. 1319-
1813
1814 631 1333.
1815
1816 632 Li, B.Y., Shen, X., Chen, G.J., Yang, Y.Q., Li, Y.S., 2012, Geochemical features of ore-
1817
1818
1819 633 forming fluids and metallogenesis of vein I₁ in Asiha gold ore deposit, Eastern Kunlun,
1820
1821
1822 634 Qinghai province: Journal of Jilin University (Earth Science Edition), v. 42, p. 1676-1687
1823
1824 635 (in Chinese with English abs.).
1825
1826
1827
1828
1829

1830
1831
1832
1833 636 Li, B.Y., Sun, F.Y., Yu, X.F., Qian, Y., Wang, G., Yang, Y.Q., 2012, U-Pb dating and
1834
1835
1836 637 geochemistry of diorite in the eastern section from eastern Kunlun middle uplifted
1837
1838 638 basement and granitic belt: *Acta Petrologica Sinica*, v. 28, p. 1163-1172 (in Chinese with
1839
1840
1841 639 English abs.).
1842
1843 640 Li, H.M., Wang, C.L., Liu, Z.W., Liu, J.Q., 2003, Two different kinds of gold deposits on
1844
1845
1846 641 northern slope of Danghenanshan area in South Qilian Mountains: *Mineral Deposits*, v.
1847
1848 642 22, p. 191-198 (in Chinese with English abs.).
1849
1850
1851 643 Li, J.C., Jia, Q.Z., Du, W., Su, Y.Z., Kong, H.L., Nan, K.E.W., Yang, B.R., 2014, LA-ICP-
1852
1853 644 MS zircon dating and geochemical characteristics of quartz diorite in Asiha gold deposit
1854
1855
1856 645 in east segment of the Eastern Kunlun: *Journal of Jilin University (Earth Science Edition)*,
1857
1858 646 v. 44, p. 1188-1199 (in Chinese with English abs.).
1859
1860
1861 647 Li, W.Y., 2008, Geochronology and geochemistry of the ophiolites and island-arc-type
1862
1863 648 igneous rocks in the Western Qinling orogen and the Eastern Kunlun orogen: implication
1864
1865
1866 649 for the evolution of the Tethyan Ocean: Ph.D. thesis, Hefei, University of Science and
1867
1868 650 Technology of China, 1-174p (in Chinese with English abs.).
1869
1870
1871 651 Liu, J., Liu, C., Carranza, E.J.M., Li, Y., Mao, Z., Wang, J., Wang, Y., Zhang, J., Zhai, D.,
1872
1873 652 Zhang, H., Shan, L., Zhu, L., Lu, R., 2015, Geological characteristics and ore-forming
1874
1875
1876 653 process of the gold deposits in the western Qinling region, China: *Journal of Asian Earth*
1877
1878 654 *Sciences*, v. 103, p. 40-69.
1879
1880
1881 655 Liu, L., Liao, X.Y., Wang, Y.W., Wang, C., Santosh, M., Yang, M., Zhang, C.L., Chen, D.L.,
1882
1883 656 2016, Early Paleozoic tectonic evolution of the North Qinling Orogenic Belt in Central
1884
1885
1886
1887
1888

1889
1890
1891
1892
1893
1894
1895
1896
1897
1898
1899
1900
1901
1902
1903
1904
1905
1906
1907
1908
1909
1910
1911
1912
1913
1914
1915
1916
1917
1918
1919
1920
1921
1922
1923
1924
1925
1926
1927
1928
1929
1930
1931
1932
1933
1934
1935
1936
1937
1938
1939
1940
1941
1942
1943
1944
1945
1946
1947

- 657 China: Insights on continental deep subduction and multiphase exhumation: Earth-
658 Science Reviews, v. 159, p. 58-81.
- 659 Liu, C.D., Zhang, W.Q., Mo, X.X., Luo, Z.H., Yu, X.H., Li, S.W., Zhao, X., 2002, Features
660 and origin of mafic microgranular enclaves in the Yuegelu granite in the Eastern Kunlun:
661 Geological Bulletin of China, v. 21, p. 739-744 (in Chinese with English abs.).
- 662 Liu, S., Li, J., Li, Y., Li, D., Zhang, A., He, S., 2016, Geochemical Characteristics of the
663 Volcanic Rocks from the Maoniushan Formation in the Dadakenwulashan Pb-Zn Deposit,
664 East Kunlun and Its Significance: Northwestern Geology, v. 49, p. 11-24 (in Chinese
665 with English abs.).
- 666 Liu, Z.Q., Pei, X.Z., Li, R.B., Li, Z.C., Zhang, X.F., Liu, Z.G., Chen, G.C., Chen, Y.X., Ding,
667 S.P., Guo, J.F., 2011, LA-ICP-MS zircon U-Pb geochronology of the two suites of
668 ophiolites at the Buqingshan area of the A'nyemaqen Orogenic Belt in the southern
669 margin of East Kunlun and its tectonic implication: Acta Geologica Sinica, v. 85, p. 185-
670 194 (in Chinese with English abs.).
- 671 Lu, L., Wu, Z.H., Hu, D.G., Patrick, J.B., Hao, S., Zhou, C.J., 2010, Zircon U-Pb age for
672 rhyolite of the Maoniushan Formation and its tectonic significance in the East Kunlun
673 Mountains: Acta Petrologica Sinica, v. 26, p. 1150-1158 (in Chinese with English abs.).
- 674 Lu, L., Zhang, Y.L., Wu, Z.H., Hu, D.G., 2013, Zircon U-Pb dating of Early Paleozoic
675 granites from the East Kunlun Mountains and its geological significance: Acta
676 Geoscientica Sinica, v. 34, p. 447-454 (in Chinese with English abs.).
- 677 Ludwig, K.R., 2012, User's manual for Isoplot 3.75—A geochronological toolkit for

1948
1949
1950
1951 678 Microsoft Excel: Berkeley, Berkeley Geochronology Center Special Publication No. 5, 1-
1952
1953
1954 679 75p.
1955
1956 680 Ma, C.Q., Xiong, F.H., Yin, S., Wang, L.X., Gao, K., 2015, Intensity and cyclicality of
1957
1958
1959 681 orogenic magmatism: An example from a Paleo-Tethyan granitoid batholith, Eastern
1960
1961 682 Kunlun, northern Qinghai-Tibetan Plateau: Acta Petrologica Sinica, v. 31, p. 3555-3568
1962
1963
1964 683 (in Chinese with English abs.).
1965
1966 684 Mao, J.W., Zhang, Z.H., Yang, J.M., Wang, Z.L., 2000, Fluid inclusions of shear zone type
1967
1968
1969 685 gold deposits in the western part of North Qilian Mountain: Mineral Deposits, v. 19, p. 9-
1970
1971 686 16 (in Chinese with English abs.).
1972
1973
1974 687 Meisel, T., Walker, R.J., Morgan, J.W., 1996, The osmium isotopic composition of the
1975
1976 688 Earth's primitive upper mantle: Nature, v. 383, p. 517-520.
1977
1978
1979 689 Meng, F.C., Cui, M.H., Wu, X.K., Wu, J.F., Wang, J.H., 2013, Magmatic and metamorphic
1980
1981 690 events recorded in granitic gneisses from the Qimantag, East Kunlun Mountains,
1982
1983
1984 691 Northwest China: Acta Petrologica Sinica, v. 29, p. 2107-2122 (in Chinese with English
1985
1986 692 abs.).
1987
1988
1989 693 Mo, X.X., Luo, Z.H., Deng, J.F., Yu, X.H., Liu, C.D., Chen, H.W., Yuan, W.M., Liu, Y.H.,
1990
1991 694 2007, Granitoids and crustal growth in the East-Kunlun Orogenic Belt: Geological
1992
1993
1994 695 Journal of China Universities, v. 13, p. 403-414 (in Chinese with English abs.).
1995
1996 696 Morelli, R., Creaser, R.A., Seltnann, R., Stuart, F.M., Selby, D., Graupner, T., 2007, Age
1997
1998
1999 697 and source constraints for the giant Muruntau gold deposit, Uzbekistan, from coupled Re-
2000
2001 698 Os-He isotopes in arsenopyrite: Geol, v. 35, p. 795.
2002
2003
2004
2005
2006

2007
2008
2009
2010
2011
2012
2013
2014
2015
2016
2017
2018
2019
2020
2021
2022
2023
2024
2025
2026
2027
2028
2029
2030
2031
2032
2033
2034
2035
2036
2037
2038
2039
2040
2041
2042
2043
2044
2045
2046
2047
2048
2049
2050
2051
2052
2053
2054
2055
2056
2057
2058
2059
2060
2061
2062
2063
2064
2065

- 699 Morelli, R.M., Bell, C.C., Creaser, R.A., Simonetti, A., 2010, Constraints on the genesis of
700 gold mineralization at the Homestake Gold Deposit, Black Hills, South Dakota from
701 rhenium-osmium sulfide geochronology: *Mineralium Deposita*, v. 45, p. 461-480.
- 702 Morelli, R.M., Creaser, R.A., Bell, C.C., 2005, Re-Os arsenopyrite geochronology of the
703 Homestake gold deposit, Black Hills, South Dakota, and implication for chronometer
704 closure temperature: Salt Lake City.
- 705 Nowell, G.M., Luguet, A., Pearson, D.G., Horstwood, M.S.A., 2008, Precise and accurate
706 $^{186}\text{Os}/^{188}\text{Os}$ and $^{187}\text{Os}/^{188}\text{Os}$ measurements by multi-collector plasma ionisation
707 mass spectrometry (MC-ICP-MS) part I: Solution analyses: *Chemical Geology*, v. 248, p.
708 363-393.
- 709 Qi, X.P., Yang, J., Fan, X.G., Cui, J.T., Cai, Z.F., Zeng, X.W., Wei, W., Qu, X.X., Zai, L.M.,
710 2016, Age, geochemical characteristics and tectonic significance of Changshishan
711 ophiolite in central East Kunlun tectonic mélangé belt along the east section of East
712 Kunlun Mountains: *Geology in China*, v. 43, p. 797-816 (in Chinese with English abs.).
- 713 Qiu, H.N., Wijbrans, J.R., 2008, The Paleozoic metamorphic history of the Central Orogenic
714 Belt of China from $^{40}\text{Ar}/^{39}\text{Ar}$ geochronology of eclogite garnet fluid inclusions: *Earth
715 and Planetary Science Letters*, v. 268, p. 501-514.
- 716 Selby, D., 2007, Direct Rhenium-Osmium age of the Oxfordian-Kimmeridgian boundary,
717 Staffin bay, Isle of Skye, U.K., and the Late Jurassic time scale: *Norwegian Journal of
718 Geology*, v. 29, p. 291-299.
- 719 Selby, D., Creaser, R.A., 2004, Macroscale NTIMS and microscale LA-MC-ICP-MS Re-Os

2066
2067
2068
2069
2070
2071
2072
2073
2074
2075
2076
2077
2078
2079
2080
2081
2082
2083
2084
2085
2086
2087
2088
2089
2090
2091
2092
2093
2094
2095
2096
2097
2098
2099
2100
2101
2102
2103
2104
2105
2106
2107
2108
2109
2110
2111
2112
2113
2114
2115
2116
2117
2118
2119
2120
2121
2122
2123
2124

720 isotopic analysis of molybdenite: Testing spatial restrictions for reliable Re-Os age
721 determinations, and implications for the decoupling of Re and Os within molybdenite:
722 *Geochimica Et Cosmochimica Acta*, v. 68, p. 3897-3908.

723 Selby, D., Creaser, R.A., Hart, C., Rombach, C.S., Thompson, J., Smith, M.T., Bakke, A.A.,
724 Goldfarb, R.J., 2002, Absolute timing of sulfide and gold mineralization: A comparison
725 of Re-Os molybdenite and Ar-Ar mica methods from the Tintina Gold Belt, Alaska:
726 *Geology*, v. 30, p. 791-794.

727 Selby, D., Kelley, K.D., Hitzman, M.W., Zieg, J., 2009, Re-Os sulfide (bornite, chalcopyrite,
728 and pyrite) systematics of the carbonate-hosted copper deposits at Ruby Creek, southern
729 Brooks range, Alaska: *Economic Geology*, v. 104, p. 437-444.

730 Shirey, S.B., Walker, R.J., 1998, The Re-Os isotope system in cosmochemistry and high-
731 temperature geochemistry: *Annual Review of Earth and Planetary Sciences*, v. 26, p.
732 423-500.

733 Song, S., Niu, Y., Su, L., Zhang, C., Zhang, L., 2014, Continental orogenesis from ocean
734 subduction, continent collision/subduction, to orogen collapse, and orogen recycling: The
735 example of the North Qaidam UHPM belt, NW China: *Earth-Science Reviews*, v. 129, p.
736 59-84.

737 Stein, H., Scherstén, A., Hannah, J., Markey, R., 2003, Subgrain-scale decoupling of Re and
738 ¹⁸⁷Os and assessment of laser ablation ICP-MS spot dating in molybdenite: *Geochimica*
739 *Et Cosmochimica Acta*, v. 67, p. 3673-3686.

740 Stein, H.J., Morgan, J.W., Scherstén, A., 2000, Re-Os dating of low-level highly radiogenic

2125
2126
2127
2128 741 (LLHR) sulfides: The Harnas gold deposit, southwest Sweden, records continental-scale
2129
2130
2131 742 tectonic events: *Economic Geology*, v. 95, p. 1657-1671.
2132
2133 743 Tao, J.J., 2014, Characteristics of fluid inclusions and genesis of Annage gold deposit,
2134
2135
2136 744 Qinghai Province: master thesis, Changsha, Central South University, 66p (in Chinese
2137
2138 745 with English abs.).
2139
2140
2141 746 Wang, G.C., Chen, N.S., Zhu, Y.H., Zhang, K.X., 2003, Late Caledonian ductile thrusting
2142
2143 747 deformation in the Central East Kunlun Belt, Qinghai, China and its significance:
2144
2145
2146 748 evidence from geochronology: *Acta Geologica Sinica*, v. 77, p. 311-319.
2147
2148
2149 749 Wang, J., Li, J., Zhao, X., Ma, C., Qu, W., Du, A., 2008, Re-Os dating of pyrrhotite from the
2150
2151 750 Chaoshan gold skarn, eastern Yangtze craton, eastern China: *International Geology*
2152
2153 751 *Review*, v. 50, p. 392-406.
2154
2155
2156 752 Wang, G., 2012, Study on geological characteristics and genesis of Guoluolongwa gold
2157
2158 753 deposit in Qinghai province: master thesis, Changchun, Jilin University, 86p (in Chinese
2159
2160
2161 754 with English abs.).
2162
2163
2164 755 Wei, B., 2015, Study on the geological characteristic and tectonic attribute of the ophiolite
2165
2166 756 and island-arc-type igneous rocks, central belt of East Kunlun (eastern section): master
2167
2168 757 thesis, Xi'an, Chang'an University, 141p (in Chinese with English abs.).
2169
2170
2171 758 Wei, X.L., Zhang, D.X., Gan, C.P., Chen, L.B., 2016, Discovery and geological significance
2172
2173 759 of Neoproterozoic intrusive body in the Kaerqueka area of the East Kunlun mountain:
2174
2175
2176 760 *Contributions to Geology and Mineral Resources Research*, v. 31, p. 236-244 (in Chinese
2177
2178 761 with English abs.).
2179
2180
2181
2182
2183

2184
2185
2186
2187 762 Wu, Y.B., Zheng, Y.F., 2013, Tectonic evolution of a composite collision orogen: An
2188
2189 763 overview on the Qinling-Tongbai-Hong'an-Dabie-Sulu orogenic belt in central China:
2190
2191
2192 764 Gondwana Research, v. 23, p. 1402-1428.
2193
2194
2195 765 Xia, R., Wang, C., Qing, M., Deng, J., Carranza, E.J.M., Li, W., Guo, X., Ge, L., Yu, W.,
2196
2197 766 2015, Molybdenite Re-Os, zircon U-Pb dating and Hf isotopic analysis of the
2198
2199 767 Shuangqing Fe-Pb-Zn-Cu skarn deposit, East Kunlun Mountains, Qinghai Province,
2200
2201
2202 768 China: Ore Geology Reviews, v. 66, p. 114-131.
2203
2204
2205 769 Xia, R., Wang, C.M., Qing, M., Li, W.L., Carranza, E.J.M., Guo, X.D., Ge, L.S., Zeng, G.Z.,
2206
2207 770 2015, Zircon U-Pb dating, geochemistry and Sr-Nd-Pb-Hf-O isotopes for the Nan'getan
2208
2209 771 granodiorites and mafic microgranular enclaves in the East Kunlun Orogen: record of
2210
2211
2212 772 closure of the Paleo-Tethys: Lithos, v. 234, p. 47-60.
2213
2214
2215 773 Xiao, Y., Feng, C.Y., Li, D.X., Liu, J.N., 2014, Chronology and fluid inclusions of the
2216
2217 774 Guoluolongwa gold deposit in Qinghai province: Acta Geologica Sinica, v. 88, p. 895-
2218
2219
2220 775 902 (in Chinese with English abs.).
2221
2222 776 Yang, J.S., Robinson, P.T., Jiang, C.F., Xu, Z.Q., 1996, Ophiolites of the Kunlun Mountains,
2223
2224
2225 777 China and their tectonic implications: Tectonophysics, v. 258, p. 215-231.
2226
2227 778 Yang, S.H., Qu, W.J., Tian, Y.L., Chen, J.F., Yang, G., Du, A.D., 2008, Origin of the
2228
2229
2230 779 inconsistent apparent Re-Os ages of the Jinchuan Ni-Cu sulfide ore deposit, China: Post-
2231
2232 780 segregation diffusion of Os: Chemical Geology, v. 247, p. 401-418.
2233
2234
2235 781 Yang, J.G., Yang, L.H., Ren, Y.X., Li, Z.P., Song, Z.B., 2005, Isotopic Geochronology of the
2236
2237 782 ore-forming process in the Hanshan gold deposit of the North Qilian Mountains: Acta
2238
2239
2240
2241
2242

2243
2244
2245
2246
2247
2248
2249
2250
2251
2252
2253
2254
2255
2256
2257
2258
2259
2260
2261
2262
2263
2264
2265
2266
2267
2268
2269
2270
2271
2272
2273
2274
2275
2276
2277
2278
2279
2280
2281
2282
2283
2284
2285
2286
2287
2288
2289
2290
2291
2292
2293
2294
2295
2296
2297
2298
2299
2300
2301

- 783 Geoscientica Sinica, v. 26, p. 315-320 (in Chinese with English abs.).
- 784 Yang, X.B., Yang, B.R., Wang, X.Y., 2006, Gold occurrence in Guoluolongwa gold deposit
785 of Qinghai Province: Geology and Prospecting, v. 42, p. 57-59 (in Chinese with English
786 abs.).
- 787 Ying, H.F., Zhang, K.X., 2003, Regional geological survey report of People's Republic of
788 China: Dongjicuonahu (I47C001002, Scale: 1:250000): Wuhan, China University of
789 Geosciences Press, 457p (in Chinese).
- 790 Yue, W.H., 2013, Geological, geochemical and genetic study of typical deposits from Gouli
791 gold field, Eastern of East Kunlun: Ph.D. thesis, Kunming, Kunming University of
792 Science and Technology, 207p (in Chinese with English abs.).
- 793 Yue, W.H., Gao, J.G., Zhou, J.X., 2013, LA-ICP-MS Zircon U-Pb Ages and
794 Litho-geochemistry of Basic Dykes in the Guoluolongwa gold ore Field, Qinghai
795 Province, China: Journal of Mineralogy and Petrology, v. 33, p. 93-102 (in Chinese with
796 English abs.).
- 797 Yue, W.H., Zhou, J.X., Gao, J.G., Huang, Y.H., Jia, F.J., 2017, Geochemistry, zircon U-Pb
798 chronology and geological implications of Sederi diabase, Dulan county, Qinghai
799 province: Bulletin of Mineralogy, Petrology and Geochemistry, v. 36, p. 270-278 (in
800 Chinese with English abs.).
- 801 Zhang, J., Ma, C., Li, J., Pan, Y., 2017, A possible genetic relationship between orogenic
802 gold mineralization and post-collisional magmatism in the eastern Kunlun Orogen,
803 western China: Ore Geology Reviews, v. 81, p. 342-357.

2302
2303
2304
2305 804 Zhang, J.Y., Ma, C.Q., Xiong, F.H., Liu, B., Li, J.W., Pan, Y.M., 2014, Early Paleozoic high-
2306
2307
2308 805 Mg diorite-granodiorite in the eastern Kunlun Orogen, western China: Response to
2309
2310 806 continental collision and slab break-off: *Lithos*, v. 210-211, p. 129-146.
2311
2312
2313 807 Zhou, Z., Mao, S., Chen, Y., Santosh, M., 2016, U-Pb ages and Lu-Hf isotopes of detrital
2314
2315 808 zircons from the southern Qinling Orogen: Implications for Precambrian to Phanerozoic
2316
2317 809 tectonics in central China: *Gondwana Research*, v. 35, p. 323-337.
2318
2319
2320 810 Zhang, D.Q., Dang, X.Y., She, H.Q., Li, D.X., Feng, C.Y., Li, J.W., 2005, Ar-Ar dating of
2321
2322
2323 811 orogenic gold deposits in northern margin of Qaidam and East Kunlun Mountains and its
2324
2325 812 geological significance: *Mineral Deposits*, v. 24, p. 87-98 (in Chinese with English abs.).
2326
2327
2328 813 Zhang, D.Q., Feng, C.Y., Li, D.X., Xu, W.Y., Yan, S.H., She, H.Q., Dong, Y.J., Cui, Y.H.,
2329
2330 814 2001, Orogenic gold deposits in the north Qaidam and East Kunlun Orogen, west China:
2331
2332 815 *Mineral Deposits*, v. 20, p. 137-146 (in Chinese with English abs.).
2333
2334
2335 816 Zhang, Y.L., Hu, D.G., Shi, Y.R., Lu, L., 2010, SHRIMP zircon U-Pb ages and tectonic
2336
2337
2338 817 significance of Maoniushan Formation volcanic rocks in East Kunlun orogenic belt,
2339
2340 818 China: *Geological Bulletin of China*, v. 29, p. 1614-1618 (in Chinese with English abs.).
2341
2342
2343 819 Zhao, C.S., 2004, Gold, silver metallogeny in Eastern Kunlun Orogenic Belt, Qinghai
2344
2345 820 province: Ph.D. thesis, Changchun, Jilin University, 144p (in Chinese with English abs.).
2346
2347
2348 821 Zhao, J.W., 2008, Study on orogenic gold metallogenic series in Eastern Kunlun Orogenic
2349
2350 822 Belt, Qinghai Province: Ph.D. thesis, Changchun, Jilin University, 189p (in Chinese with
2351
2352
2353 823 English abs.).
2354
2355 824 Zhu, Y.H., Pan, Y.M., Zhang, K.X., Chen, N.S., Wang, G.C., Hou, G.J., 2000, Mineralogical
2356
2357
2358
2359
2360

2361
2362
2363
2364
2365
2366
2367
2368
2369
2370
2371
2372
2373
2374
2375
2376
2377
2378
2379
2380
2381
2382
2383
2384
2385
2386
2387
2388
2389
2390
2391
2392
2393
2394
2395
2396
2397
2398
2399
2400
2401
2402
2403
2404
2405
2406
2407
2408
2409
2410
2411
2412
2413
2414
2415
2416
2417
2418
2419

- 825 characteristics and petrogenesis of ophiolites in East Kunlun Orogenic Belt, Qinghai
Province: *Acta Mineralogica Sinica*, v. 20, p. 128-142 (in Chinese with English abs.).
- 826

2420
2421
2422
2423
2424
2425
2426
2427
2428
2429
2430
2431
2432
2433
2434
2435
2436
2437
2438
2439
2440
2441
2442
2443
2444
2445
2446
2447
2448
2449
2450
2451
2452
2453
2454
2455
2456
2457
2458
2459
2460
2461
2462
2463
2464
2465
2466
2467
2468
2469
2470
2471
2472
2473
2474
2475
2476
2477
2478

827 **Figure captions**

828 **Fig. 1** (A) Tectonic map of China showing the location of Central Orogenic Belt and
829 significant gold producing areas (after [Li et al., 2015](#)). (B) Tectonic divisions of the Qinghai-
830 Tibetan plateau showing the location of the East Kunlun Orogen (after [Xia et al., 2015](#)). (C)
831 Simply Geological map of the East Kunlun Orogen showing the main gold deposits/fields
832 (after [Xia et al., 2015](#)).

834 **Fig. 2** Geological map of the Gouli goldfield showing the distribution of the main gold
835 deposits (after unpublished geological report). Ages labeled on the map are zircon U-Pb ages
836 and the related references are as follows: (1) ([Chen et al., 2012](#)); (2) ([Liu et al., 2002](#)); (3)
837 (J.J. Chen et al. in prep.); (4) ([Ying and Zhang, 2003](#)); (5) (our unpublished data); (6) ([Chen](#)
838 [et al., 2016](#)); (7) (our unpublished data); (8) ([Li et al., 2012](#)); (9) ([Yue et al., 2017](#)); (10)
839 ([Chen et al., 2006](#)).

841 **Fig. 3** (A) Geological map of the Guoluolongwa gold deposit showing the locations of the
842 main gold orebodies and the profile A-B. (B) Representative cross-section in the
843 Guoluolongwa gold deposit (after unpublished geological report). Ages in (A) are zircon U-
844 Pb ages from our unpublished data and [Yue et al. \(2013\)](#).

846 **Fig. 4** (A) Geological map of the Annage gold deposit showing the distribution of the main
847 gold orebodies and the location of profile A-B (after [Chen, 2014](#)). (B) Representative cross-

2479
2480
2481
2482
2483
2484
2485
2486
2487
2488
2489
2490
2491
2492
2493
2494
2495
2496
2497
2498
2499
2500
2501
2502
2503
2504
2505
2506
2507
2508
2509
2510
2511
2512
2513
2514
2515
2516
2517
2518
2519
2520
2521
2522
2523
2524
2525
2526
2527
2528
2529
2530
2531
2532
2533
2534
2535
2536
2537

848 section in the Annage gold deposit (after unpublished geological report). Age of diorite in (A)
849 is zircon U-Pb age from Kong et al. (2014).

850
851 **Fig. 5** Photographs and photomicrographs showing representative veins and minerals in the
852 Guoluolongwa (A-I) and Annage (J-L) gold deposits. (A) Crosscutting relationship of the
853 pyrite-quartz vein, polymetallic sulfides-quartz vein, gabbro, and phyllite. (B) Pyrite-quartz
854 vein cutting cross early quartz vein. (C) Polymetallic sulfides-quartz ore. (D) Native gold-
855 chalcopyrite-sphalerite vein filling the crack of pyrite. (E) Native gold occurring between
856 sphalerite and quartz grains. (F) Chalcopyrite-galena vein; (G) Eutectoid of sphalerite and
857 chalcopyrite. (H) Polymetallic sulfides-quartz vein cut cross early pyrite-quartz vein. (I)
858 Polymetallic sulfides-quartz vein. (J) Pyrite-quartz vein with local massive pyrite. (K) Pyrite-
859 quartz ore. (L) Coarse pyrite.

860
861 **Fig. 6** Mineral paragenetic sequence of Guoluolongwa and Annage deposits.

862
863 **Fig. 7** Re-Os plots of stage II pyrite-quartz vein in the Guoluolongwa gold deposit: (A)
864 $^{187}\text{Re}/^{188}\text{Os}$ vs. $^{187}\text{Os}/^{188}\text{Os}$ plot; (B) ^{187}Re vs. $^{187}\text{Os}^r$ plot; (C) Weight average of Re-Os model
865 dates.

866

2538
2539
2540
2541
2542
2543
2544
2545
2546
2547
2548
2549
2550
2551
2552
2553
2554
2555
2556
2557
2558
2559
2560
2561
2562
2563
2564
2565
2566
2567
2568
2569
2570
2571
2572
2573
2574
2575
2576
2577
2578
2579
2580
2581
2582
2583
2584
2585
2586
2587
2588
2589
2590
2591
2592
2593
2594
2595
2596

Fig. 8 Re-Os plots of stage III polymetallic sulfides-quartz vein in the Guoluolongwa gold deposit: (A) $^{187}\text{Re}/^{188}\text{Os}$ vs. $^{187}\text{Os}/^{188}\text{Os}$ plot; (B) ^{187}Re vs. $^{187}\text{Os}^r$ plot; (C) Weight average of Re-Os model dates.

Fig. 9 Re-Os plots of stage gold-bearing vein in the Annage gold deposit: (A) $^{187}\text{Re}/^{188}\text{Os}$ vs. $^{187}\text{Os}/^{188}\text{Os}$ plot; (B) ^{187}Re vs. $^{187}\text{Os}^r$ plot; (C) Weight average of Re-Os model dates.

Fig. 10 Initial $^{187}\text{Os}/^{188}\text{Os}$ vs. T (Ma) of sulfides from the Guoluolongwa (A, B) and Annage (C) gold deposits. The number “48” overriding the grey lines is the present-day continental crustal $^{187}\text{Re}/^{188}\text{Os}$ value used for calculating evolution lines of crust with different ages (Esser and Turekian, 1993). The numbers 300 and 500 overriding orange lines are assumed present-day $^{187}\text{Re}/^{188}\text{Os}$ values used for calculating corresponding crustal evolution lines. Present-day $^{187}\text{Os}/^{188}\text{Os}$ and $^{187}\text{Re}/^{188}\text{Os}$ values used for calculating the primitive upper mantle evolution line are 0.1290 and 0.428, respectively (Meisel et al., 1996). Os composition of the Ordovician black shales is also shown for comparison (Finlay et al., 2010). The initial $^{187}\text{Os}/^{188}\text{Os}$ ratios present here are from samples with $\%^{187}\text{Os}^r < 90\%$.

Fig. 11 initial $^{187}\text{Os}/^{188}\text{Os}$ vs. $1/\text{Os}$ of sulfides from Guoluolongwa (A, B) and Annage (C) gold deposits. The initial $^{187}\text{Os}/^{187}\text{Os}$ ratios used were calculated back to 202.7 Ma (Xiao et al., 2014).

2597
2598
2599
2600
2601
2602
2603
2604
2605
2606
2607
2608
2609
2610
2611
2612
2613
2614
2615
2616
2617
2618
2619
2620
2621
2622
2623
2624
2625
2626
2627
2628
2629
2630
2631
2632
2633
2634
2635
2636
2637
2638
2639
2640
2641
2642
2643
2644
2645
2646
2647
2648
2649
2650
2651
2652
2653
2654
2655

888 **Fig. 12** H-O isotopic characteristics of Guoluolongwa and Annage gold deposits. The H-O
889 isotopic data of the Guoluolongwa and Annage gold deposit are from Yue (2013), Xiao et al.
890 (2014), Wang (2012), Hu (2008) and Tao (2014). H-O isotopic data of gold deposits from the
891 East Kunlun Orogen (Feng et al., 2004; Zhao, 2008; Li et al., 2012; Tao, 2014), western
892 Qinling (Liu et al., 2015 and references therein) and Qaidam-Qilian (Mao et al., 2000; Li et
893 al., 2003; Fan et al., 2006; Ding, 2007) are also shown for comparison. GLLW-
894 Guoluolongwa gold deposit; ANG- Annage gold deposit; EKO- East Kunlun Orogen.

895
896 **Fig. 13** Temporal distribution of gold deposits from East Kunlun Orogen, western Qinling
897 and Qaidam-Qilian. A-type granites and related mafic rocks from East Kunlun Orogen are
898 also shown indicating post-collisional extensional setting for gold deposits. The period of
899 collision/post-collision of the East Kunlun Orogen (Chen et al., 2017; Chen et al., in
900 preparation), western Qinling (Liu et al., 2016; Zhou et al., 2016) and Qaidam-Qilian (Song
901 et al., 2014) are also marked. The sources of ages of gold deposits, A-type granites, and
902 related mafic rocks are summarized in the appendix.

Fig. 1

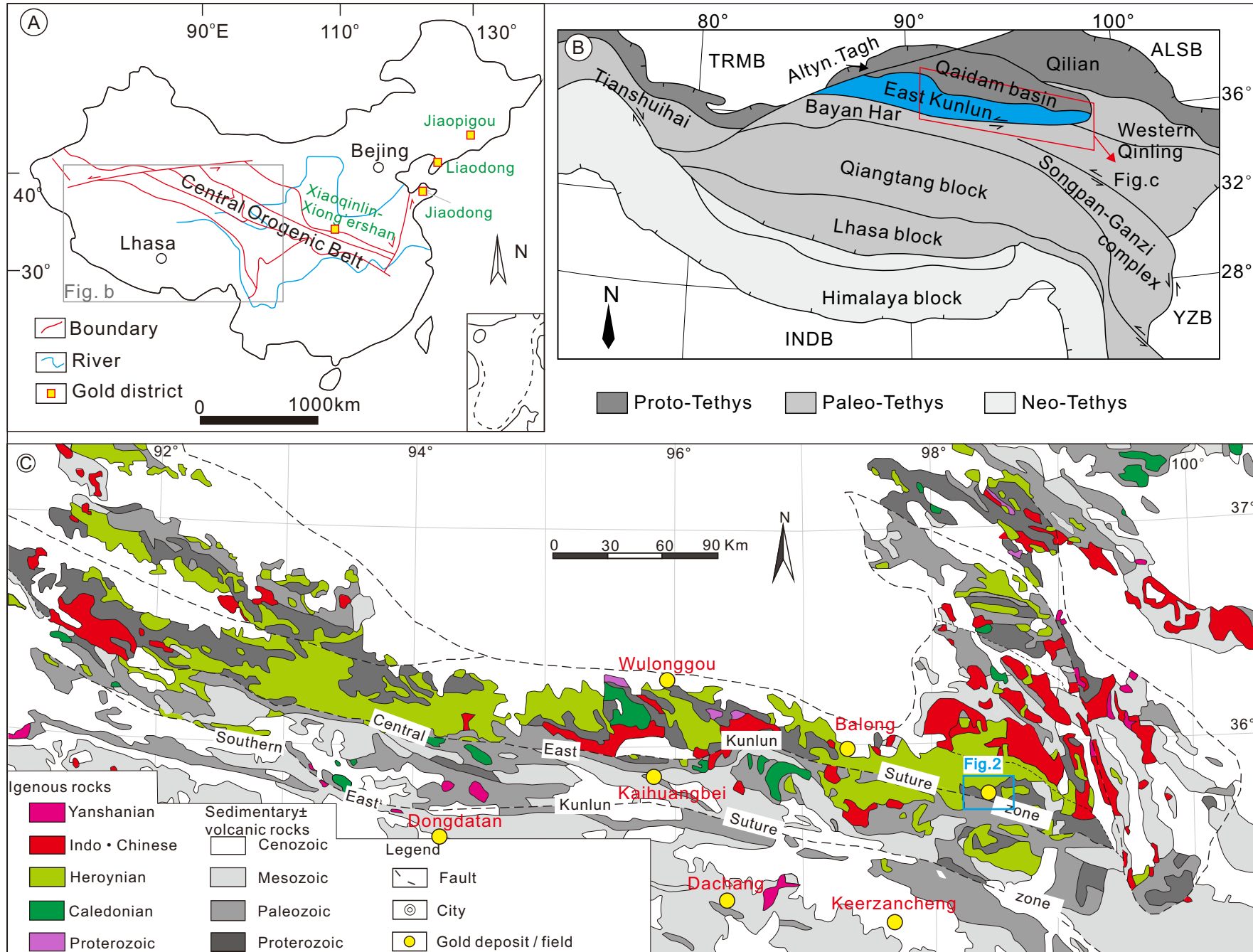
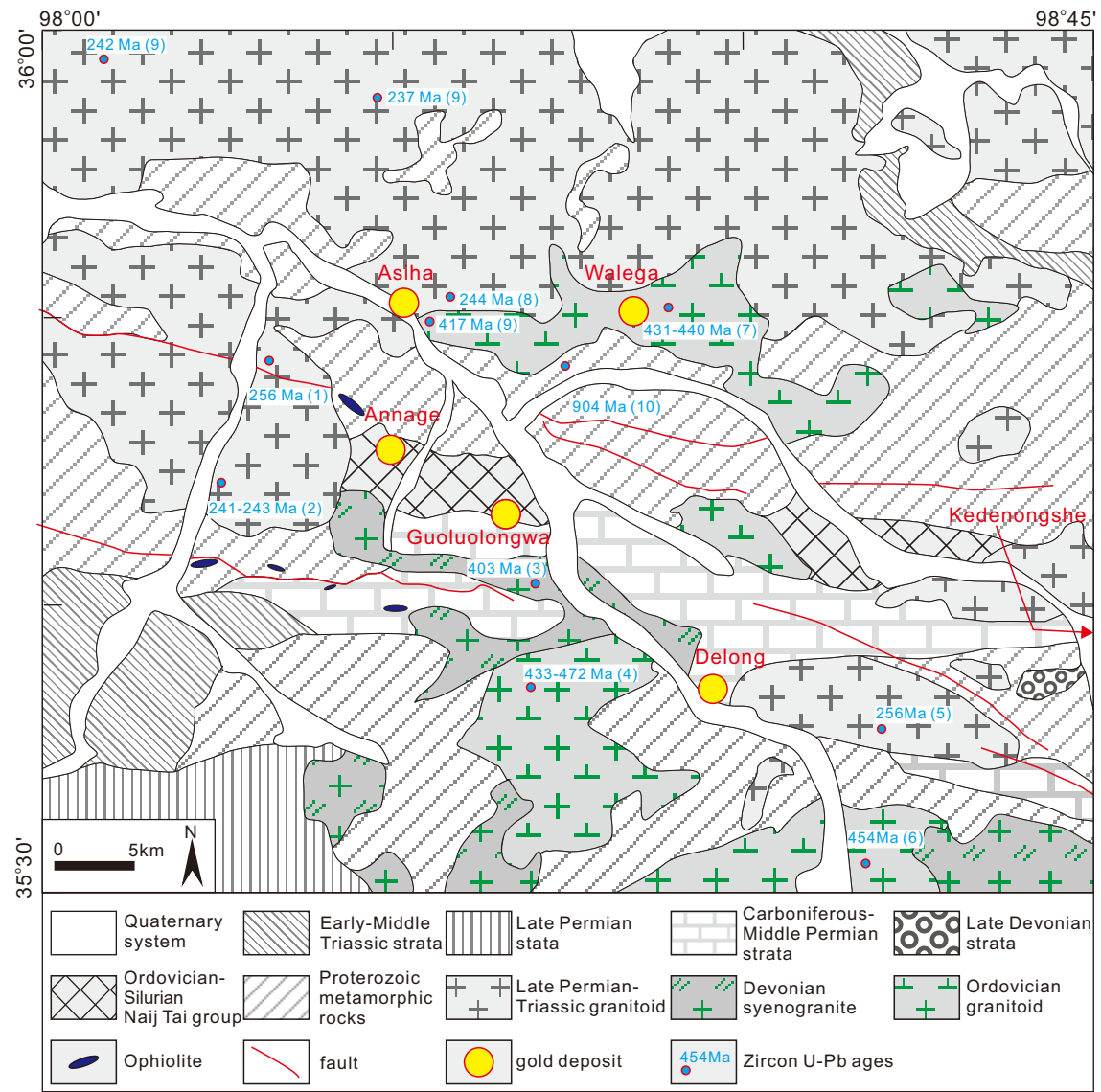


Fig. 2



1
2
3
4
5
6
7
8
9
10
11
12
13
14
15
16
17
18
19
20
21
22
23
24
25
26
27
28
29
30
31
32
33
34
35
36
37
38
39
40
41
42
43
44
45
46
47
48
49
50
51
52
53
54
55
56
57
58
59

Fig. 3

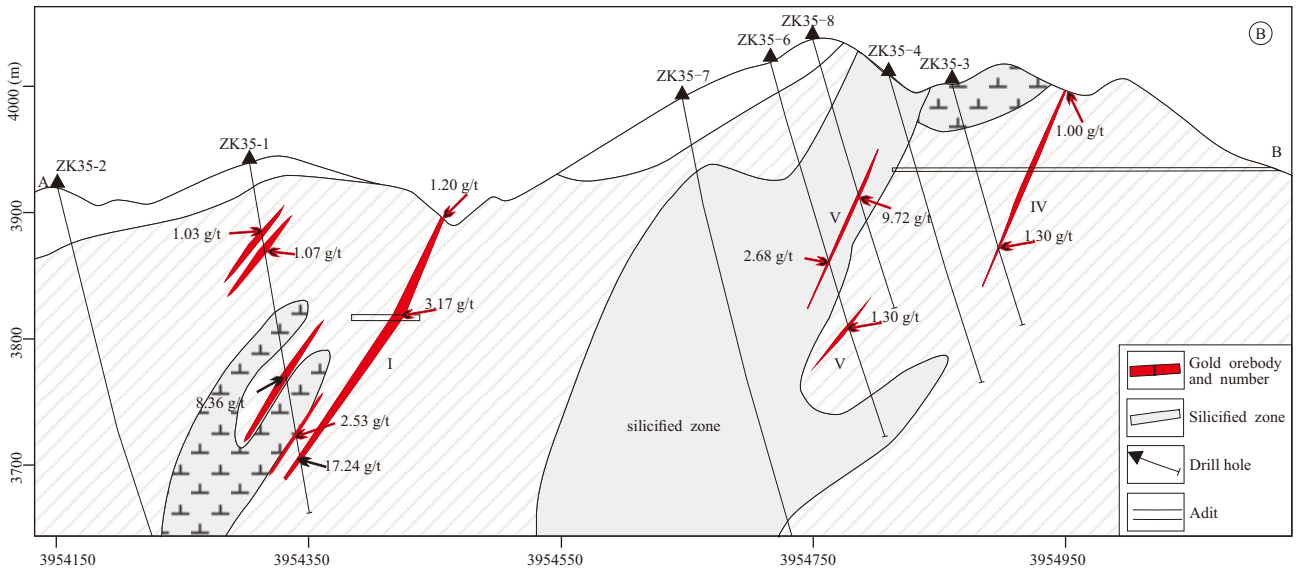
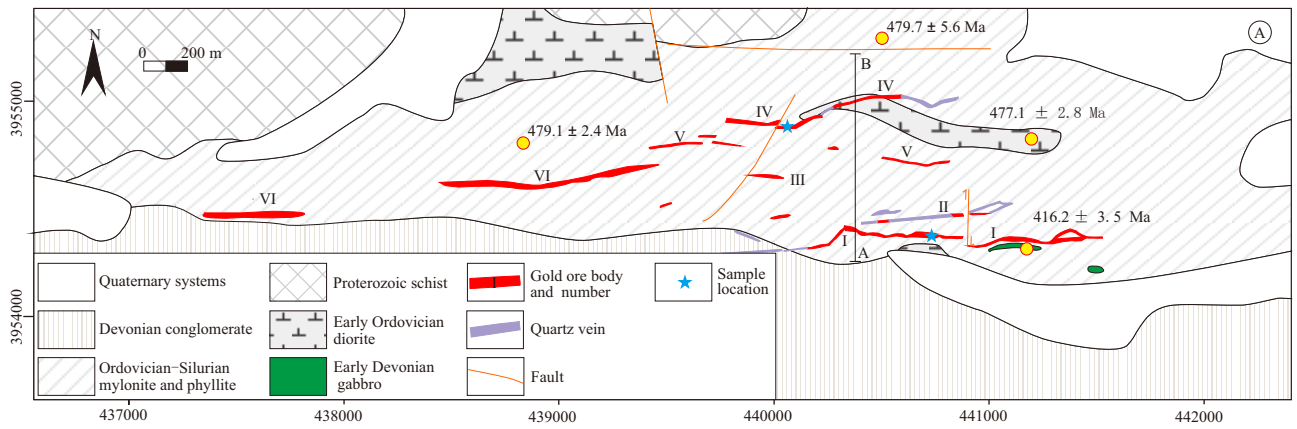
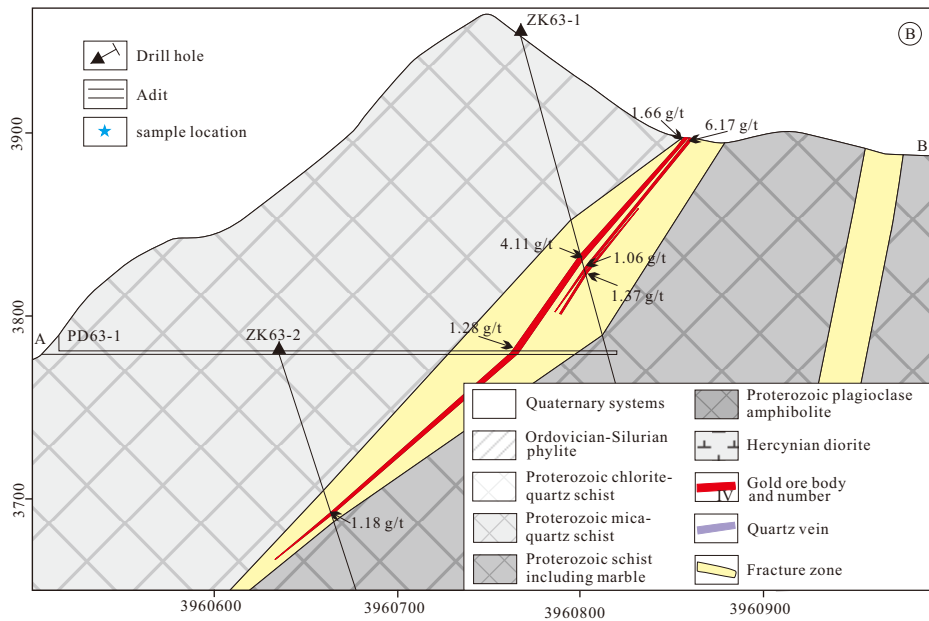
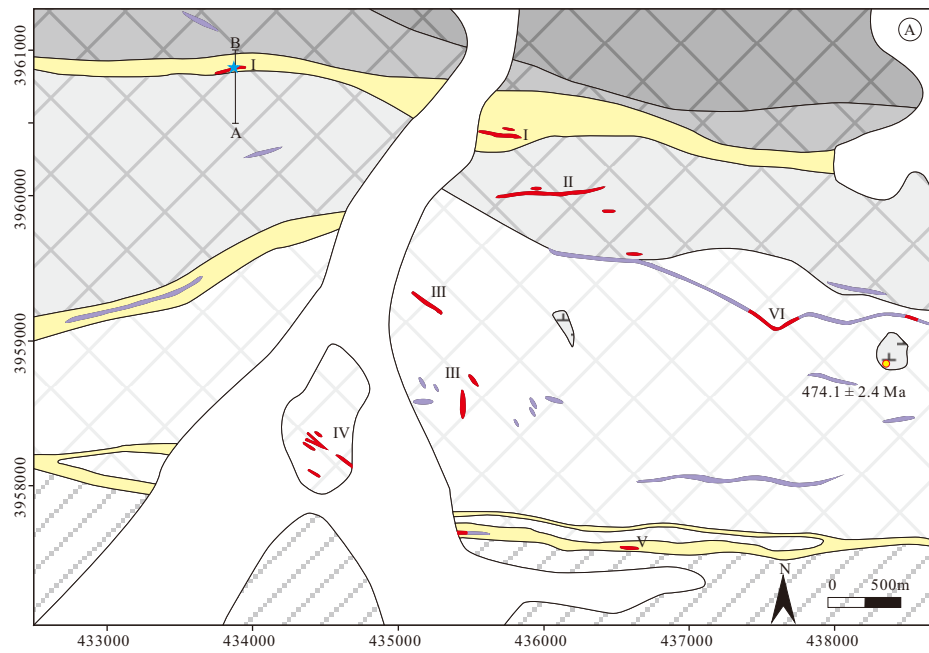
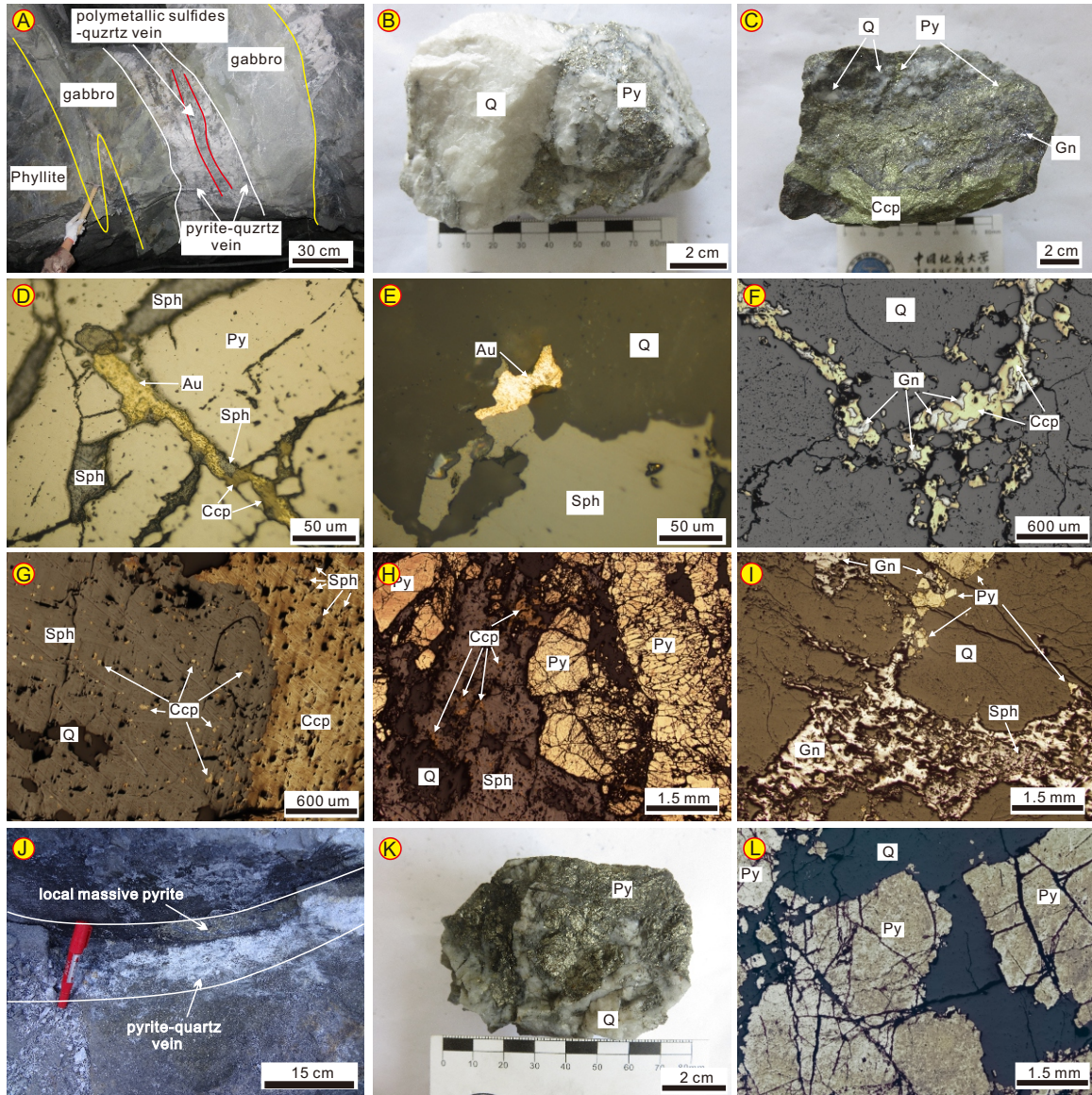


Fig. 4



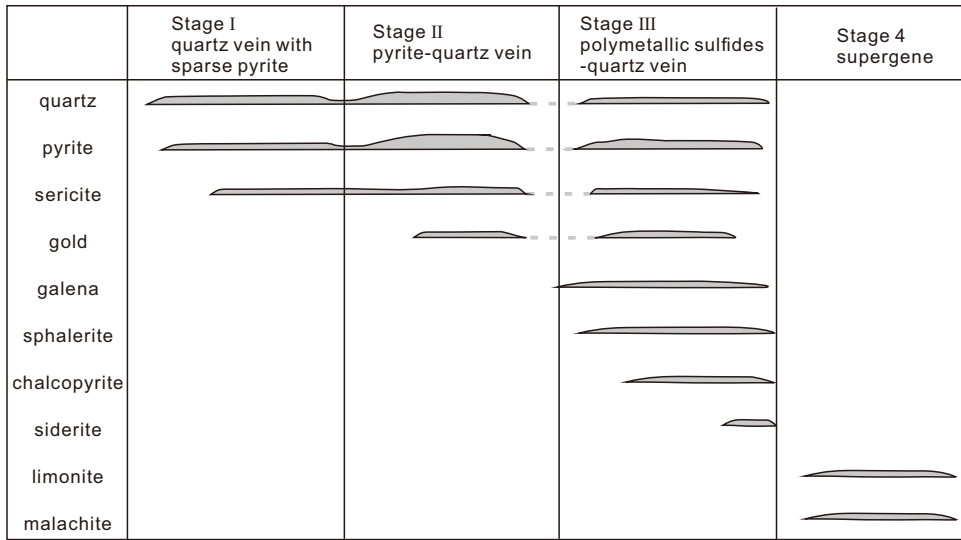
1
2
3
4
5
6
7
8
9
10
11
12
13
14
15
16
17
18
19
20
21
22
23
24
25
26
27
28
29
30
31
32
33
34
35
36
37
38
39
40
41
42
43
44
45
46
47
48
49
50
51
52
53
54
55
56
57
58
59

Fig. 5



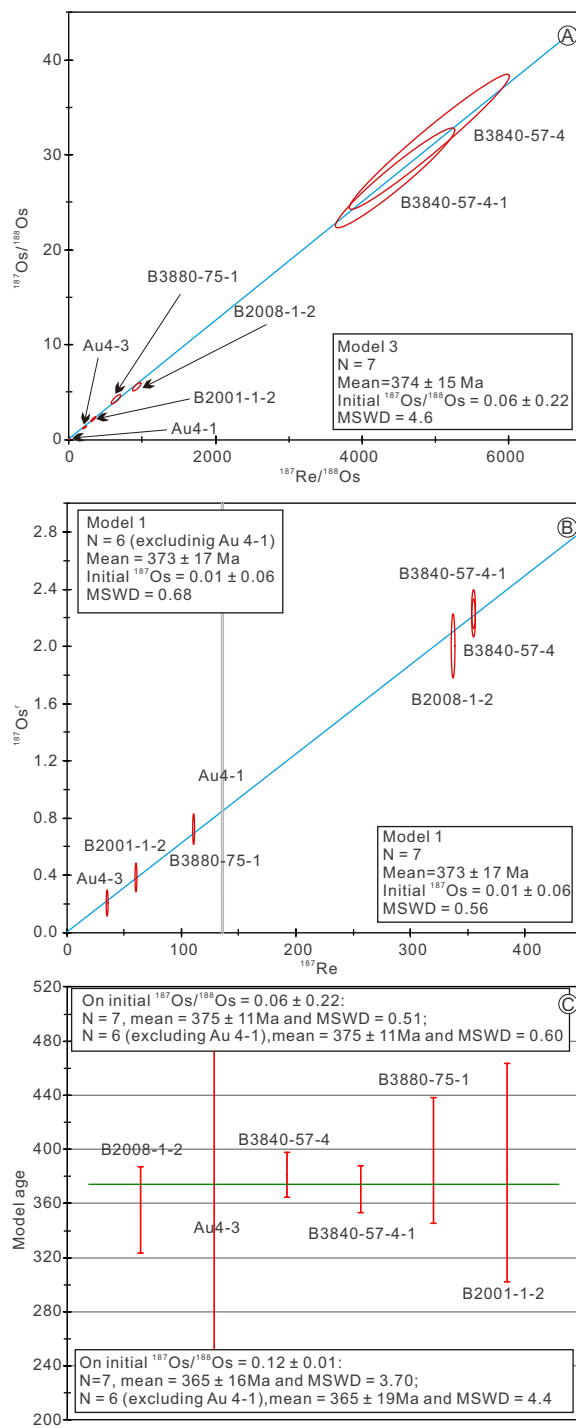
1
2
3
4
5
6
7
8
9
10
11
12
13
14
15
16
17
18
19
20
21
22
23
24
25
26
27
28
29
30
31
32
33
34
35
36
37
38
39
40
41
42
43
44
45
46
47
48
49
50
51
52
53
54
55
56
57
58
59

Fig. 6



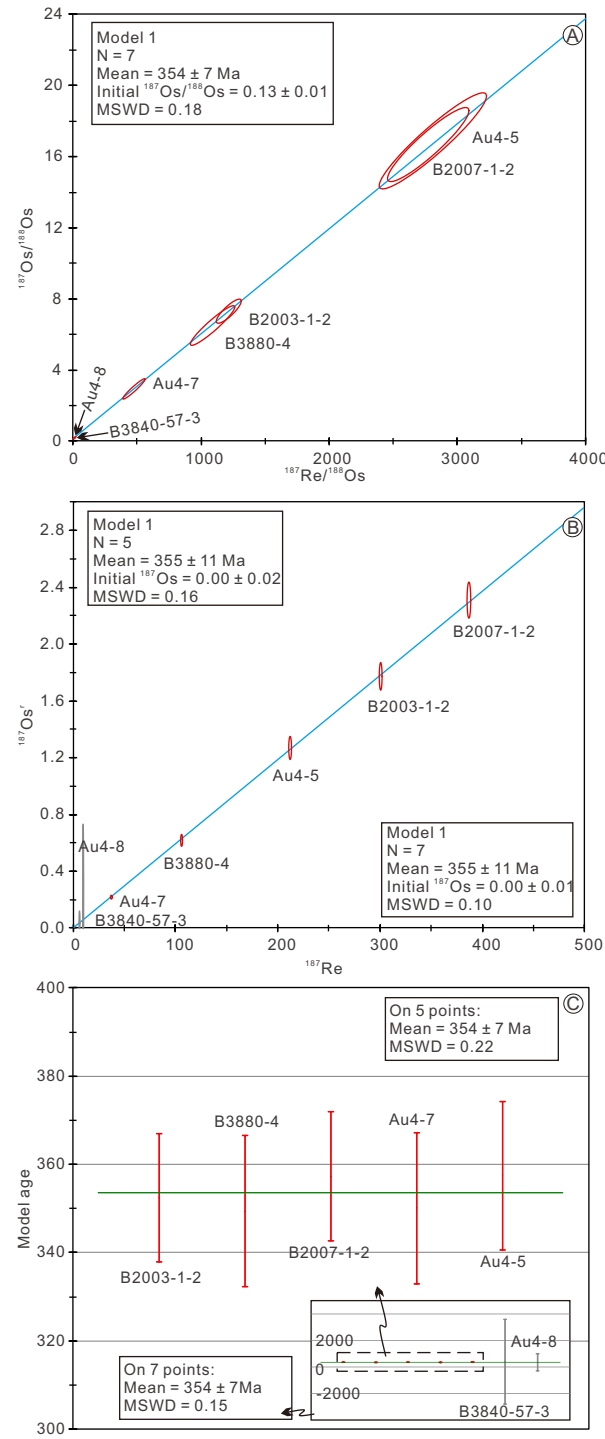
1
2
3
4
5
6
7
8
9
10
11
12
13
14
15
16
17
18
19
20
21
22
23
24
25
26
27
28
29
30
31
32
33
34
35
36
37
38
39
40
41
42
43
44
45
46
47
48
49
50
51
52
53
54
55
56
57
58
59

Fig. 7



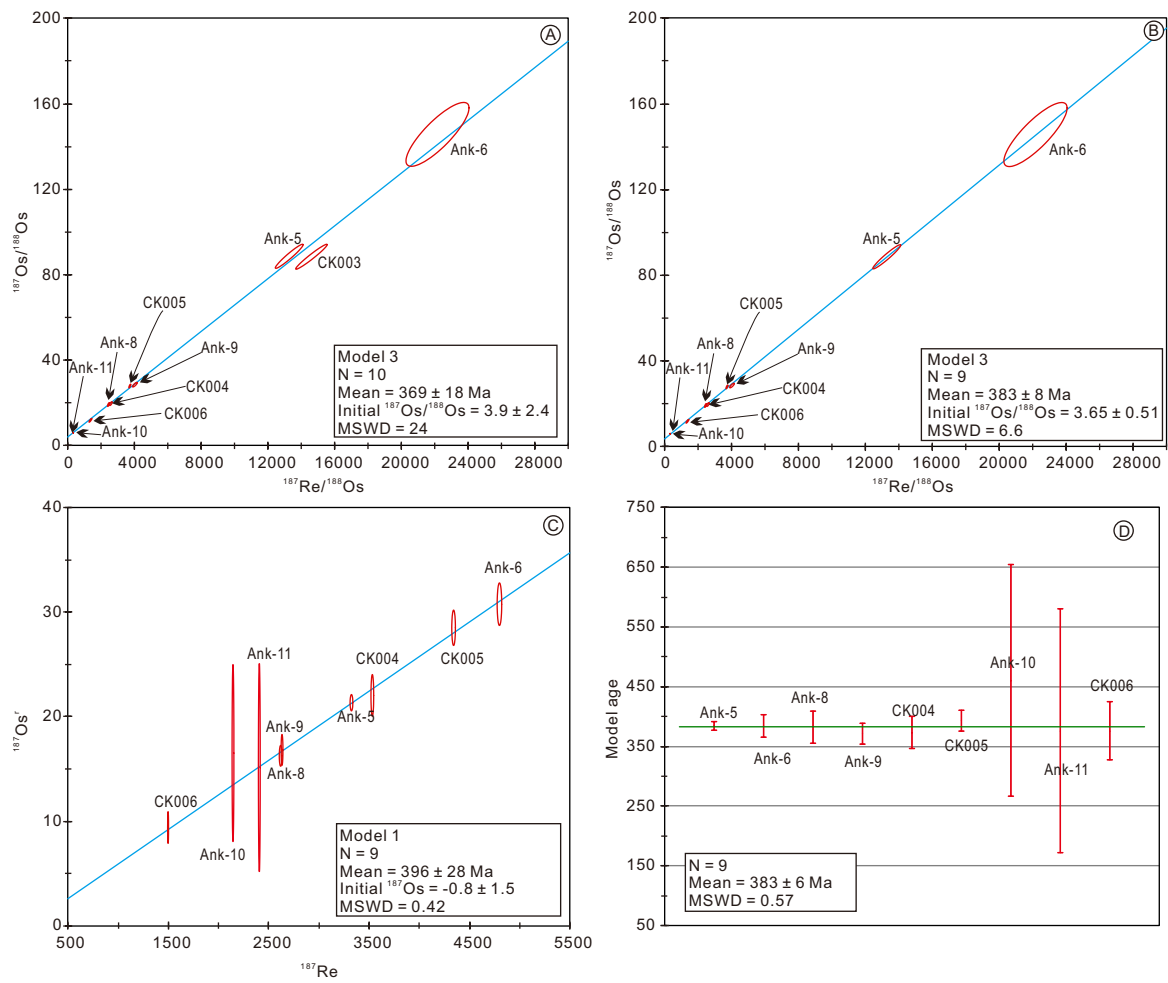
1
2
3
4
5
6
7
8
9
10
11
12
13
14
15
16
17
18
19
20
21
22
23
24
25
26
27
28
29
30
31
32
33
34
35
36
37
38
39
40
41
42
43
44
45
46
47
48
49
50
51
52
53
54
55
56
57
58
59

Fig. 8



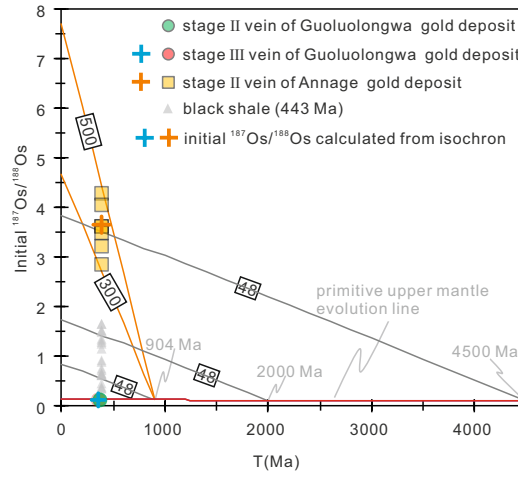
1
2
3
4
5
6
7
8
9
10
11
12
13
14
15
16
17
18
19
20
21
22
23
24
25
26
27
28
29
30
31
32
33
34
35
36
37
38
39
40
41
42
43
44
45
46
47
48
49
50
51
52
53
54
55
56
57
58
59

Fig. 9



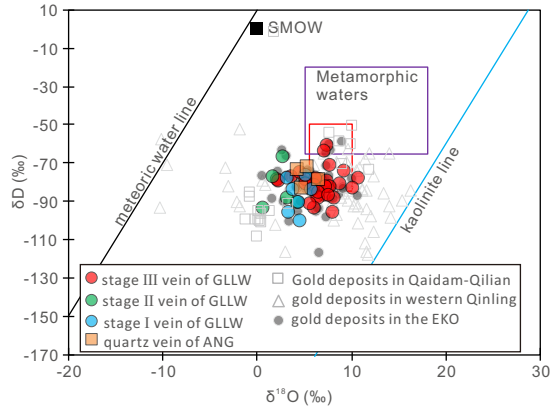
1
2
3
4
5
6
7
8
9
10
11
12
13
14
15
16
17
18
19
20
21
22
23
24
25
26
27
28
29
30
31
32
33
34
35
36
37
38
39
40
41
42
43
44
45
46
47
48
49
50
51
52
53
54
55
56
57
58
59

Fig. 10



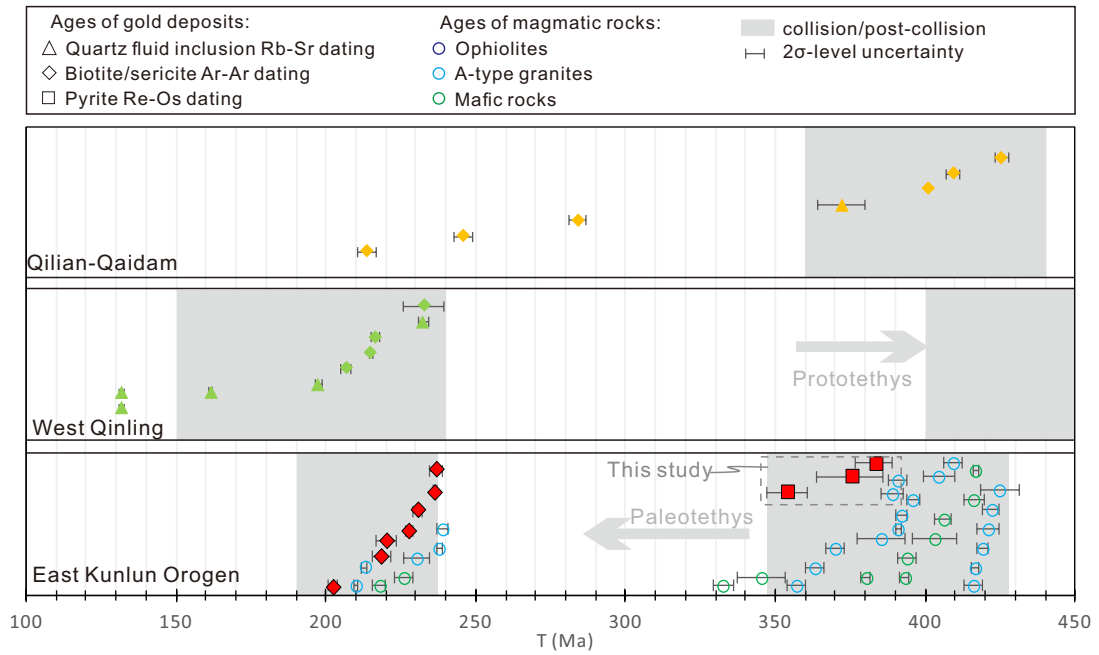
1
2
3
4
5
6
7
8
9
10
11
12
13
14
15
16
17
18
19
20
21
22
23
24
25
26
27
28
29
30
31
32
33
34
35
36
37
38
39
40
41
42
43
44
45
46
47
48
49
50
51
52
53
54
55
56
57
58
59

Fig. 12



1
2
3
4
5
6
7
8
9
10
11
12
13
14
15
16
17
18
19
20
21
22
23
24
25
26
27
28
29
30
31
32
33
34
35
36
37
38
39
40
41
42
43
44
45
46
47
48
49
50
51
52
53
54
55
56
57
58
59

Fig. 13



1
2
3
4
5
6
7
8
9
10
11
12
13
14
15
16
17
18
19
20
21
22
23
24
25
26
27
28
29
30
31
32
33
34
35
36
37
38
39
40
41
42
43
44
45
46
47
48
49
50
51
52
53
54
55
56
57
58
59

Appendix table A1 Typical gold deposits in the west of the Central Orogenic Belt of China

deposit	resources (t)	Tectonic terrain	mineralization age (Ma)	mineral and method	reference
Hanshan		Qilian	372 ± 8 ; 213.9 ± 3.1	Quartz, Rb-Sr; Sericite, K-Ar	(Mao et al., 2000; Yang et al., 2005)
Yeluotuoquan		Qaidam	246 ± 3	Sericite, Ar-Ar	(Zhang et al., 2005)
Tanjianshan		Qaidam	284 ± 3 ; 401	Sericite and biotite, Ar-Ar;	(Zhang et al., 2005)
Qinglonggou		Qaidam	409.4 ± 2.3	Sericite, Ar-Ar	(Zhang et al., 2005)
Saibagou		Qaidam	425.5 ± 2.1	Sericite, Ar-Ar	(Zhang et al., 2005)
Wulonggou	72.93	East Kunlun Orogen	236.5 ± 0.5	Sericite, Ar-Ar	(Zhang et al., 2005)
Shuizhadonggou	45.00	East Kunlun Orogen	230.8 ± 1.7 ; 237 ± 2	Sericite, Ar-Ar	(Zhang et al., 2017)
Huanglonggou					
Guoluolongwa	40.00	East Kunlun Orogen	202.7 ± 1.5	Sericite, Ar-Ar	(Xiao et al., 2014)
Dachang	220.00	East Kunlun Orogen	218.6 ± 3.2 ; 220.3 ± 3.2	Sericite, Ar-Ar	(Feng, 2002; Zhang et al., 2005)
Naomuhun		East Kunlun Orogen	227.84 ± 1.13	Sericite, Ar-Ar	(Li et al., 2017)
Guoluolongwa	40.00	East Kunlun Orogen	202.7 ± 1.5 ; 375 ± 11 ; 354 ± 7	Pyrite, Re-Os	(Xiao et al., 2014; This study)
Annage		East Kunlun Orogen	383 ± 6	Pyrite, Re-Os	This study
Baguamiao	106.00	western Qinling	232.58 ± 1.59 ; 131.9 ± 0.98 ; 131.91 ± 0.89	Quartz, Ar-Ar	(Shao and Wang, 2001)
Xiaogouli		western Qinling	197.45 ± 1.13	Quartz, Ar-Ar	(Shao and Wang, 2001)
Shangjiagou		western Qinling	161.59 ± 0.56	Quartz, Ar-Ar	(Shao and Wang, 2001)
Liziyuan		western Qinling	206.8 ± 1.6	Sericite, K-Ar	(Liu et al., 2011)
Liba	80.00	western Qinling	216.4 ± 1.5	Muscovite and biotite, Ar-Ar	(Zeng et al., 2012)
Huachanggou	10.00	western Qinling	215 ± 0.5	Fuchsite, K-Ar	(Bai, 1996)

42
43
44
45
46
47
48
49
50
51
52
53
54
55
56
57
58
59
60
61
62
63
64
65
66
67
68
69
70
71
72
73
74
75
76
77
78
79
80
81
82

Jinlongshan	>150	western Qinling	232.7 ± 6.9	Sericite, Ar–Ar	(Zhao et al., 2001)
Yangshan	>300	western Qinling	197.6 ± 1.7	Zircon, U-Pb (SHRIMP)	(Qi et al., 2005)

Appendix table A2 A-type granites and related mafic rocks in the East Kunlun Orogen

Location	lithology	age (Ma)	method	references
Yugouzi	A-type granite	210 ± 0.6	Zircon LA-ICPMS U-Pb	(Gao, 2013)
Yemaquan	A-type granite	213 ± 1	Zircon LA-ICPMS U-Pb	(Gao et al., 2014)
Kendekeke	A-type granite	230.5 ± 4.2	Zircon LA-ICPMS U-Pb	(Xi et al., 2010)
Baishiya	A-type granite	238 ± 1	Zircon LA-ICPMS U-Pb	(Yin et al., 2013)
Halashan	A-type granite	239.2 ± 1.7	Zircon LA-ICPMS U-Pb	(He, 2015)
Tula	A-type granite	385.2 ± 8.1	Zircon SHRIMP U-Pb	(Wu et al., 2007)
Wulanwuzhuer	A-type granite	388.9 ± 3.7	Zircon LA-ICPMS U-Pb	(Guo et al., 2011)
Binggou	A-type granite	391 ± 3	Zircon LA-ICPMS U-Pb	(Liu et al., 2013)
Xiarhamu	A-type granite	391 ± 1	Zircon LA-ICPMS U-Pb	(Wang et al., 2013)
Dagangou	A-type granite	392 ± 2	Zircon LA-ICPMS U-Pb	(Tian et al., 2016)
Lalingzaohuo	A-type granite	396 ± 2	Zircon LA-ICPMS U-Pb	(Chen et al., 2013)
Shuizhadonggou	A-type granite	404.6 ± 5.2	Zircon LA-ICPMS U-Pb	(Wang, 2015)
Shuizhadonggou	A-type granite	409.3 ± 2.8	Zircon LA-ICPMS U-Pb	(Wang, 2015)
Dacaigou	A-type granite	416 ± 3	Zircon LA-ICPMS U-Pb	(Wang, 2015)
Huanglonggou	A-type granite	416.9 ± 1.3	Zircon LA-ICPMS U-Pb	(Li et al., 2014)
Houtougou	A-type granite	419 ± 1.9	Zircon LA-ICPMS U-Pb	(Yan et al., 2016)
Baiganhu	A-type granite	421 ± 3.7	Zircon SHRIMP U-Pb	(Li et al., 2012)
Baiganhu	A-type granite	422 ± 3	Zircon SHRIMP U-Pb	(Li et al., 2012)
Helegangnaren	A-type granite	425 ± 6.7	Zircon LA-ICPMS U-Pb	(Li et al., 2013)
Zongjia	basic dike	218±2	Zircon LA-ICPMS U-Pb	(Xiong, 2014)

83
84
85
86
87
88
89
90
91
92
93
94
95
96
97
98
99
100
101
102
103
104
105
106
107
108
109
110
111
112
113
114
115
116
117
118
119
120
121
122
123

Binggou	basic dike	226±3	Zircon LA-ICPMS U-Pb	(Xiong, 2014)
Qimantage	dolerite	380.3 ± 1.5	Zircon LA-ICPMS U-Pb	(Qi et al., 2013)
East of Yuejinshan	hornblende gabbro	393.1 ± 1.6	Zircon LA-ICPMS U-Pb	(Xiong et al., 2014)
Xiarihamu	gabbro	394 ± 3	Zircon LA-ICPMS U-Pb	(Li et al., 2012)
Geyakedengtage	gabbro	403.3 ± 7.2	Zircon SHRIMP U-Pb	(Chen et al., 2006)
Yuejinshan	gabbro	406 ± 3	Zircon LA-ICPMS U-Pb	(Liu et al., 2012)
Guoluolongwa	lamprophyre	416.3 ± 3.5	Zircon LA-ICPMS U-Pb	(Yue et al., 2013)
Sederi	dolerite	417 ± 1	Zircon LA-ICPMS U-Pb	(Yue et al., 2017)
Haerguole	gabbro from ophiolite	332.8 ± 3.1	Zircon LA-ICPMS U-Pb	(Liu et al., 2011)
Xiadawu	gabbro from ophiolite	345.3 ± 7.9	whole rock Ar-Ar	(Chen et al., 2001)

REFERENCES

Chen, L., Sun, Y., Pei, X.Z., Gao, M., Tao, F., Zhang, Z.Q., Chen, W., 2001, Northernmost Paleo-Tethyan oceanic basin in Tibet: geochronological evidence from $^{40}\text{Ar}/^{39}\text{Ar}$ age dating of Dur'ngoi ophiolite: Chinese Science Bulletin, v. 46, p. 1203-1205.

Li, R.B., Pei, X.Z., Li, Z.C., Sun, Y., Pei, L., Chen, G.C., Chen, Y.X., Liu, C.J., Wei, F.H., 2013, Regional tectonic transformation in East Kunlun Orogenic Belt in Early Paleozoic: constraints from the geochronology and geochemistry of Helegangnaren alkali-feldspar granite: Acta Geologica Sinica, v. 87, p. 333-345.

Xiong, F.H., Ma, C.Q., Jiang, H.A., Liu, B., Huang, J., 2014, Geochronology and geochemistry of Middle Devonian mafic dykes in the East

124
125
126
127
128 Kunlun orogenic belt, Northern Tibet Plateau: Implications for the transition from Prototethys to Paleotethys orogeny: *Chemie der Erde -*
129
130
131 *Geochemistry*, v. 74, p. 225-235.

132
133 Zeng, Q.T., McCuaig, T.C., Hart, C.J.R., Jourdan, F., Muhling, J., Bagas, L., 2012, Structural and geochronological studies on the Liba goldfield
134
135 of the West Qinling Orogen, Central China: *Mineralium Deposita*, v. 47, p. 799-819.

136
137 Zhang, J.Y., Ma, C.Q., Li, J.W., Pan, Y.M., 2017, A possible genetic relationship between orogenic gold mineralization and post-collisional
138
139 magmatism in the eastern Kunlun Orogen, western China: *Ore Geology Reviews*, v. 81, Part 1, p. 342-357.

140
141 Bai, Z., 1996, Genesis of the Huachanggou gold deposit in Shanxi Province: *Mineral Resources and Geology*, v. 10, p. 108-113 (in Chinese with
142
143 English abs.).

144
145
146
147
148 Chen, J., Xie, Z.Y., Li, B., Tan, S.X., Ren, H., Zhang, Q.M., Li, Y., 2013, Petrogenesis of Devonian intrusive rocks in Lalingzaohuo area,
149
150 Eastern Kunlun, and its geological significance: *Journal of Mineralogy and Petrology*, v. 33, p. 26-34 (in Chinese with English abs.).

151
152
153 Chen, H.W., Luo, Z.H., Mo, X.X., Zhang, X.T., Wang, J., Wang, B.Z., 2006, SHRIMP ages of Kayakedengtage complex in the East Kunlun
154
155 Mountains and their geological implications: *Acta Petrologica Et Mineralogica*, v. 25, p. 25-32 (in Chinese with English abs.).

156
157
158 Feng, C.Y., 2002, Multiple orogenic processes and mineralization of orogenic gold deposits in the East Kunlun Orogen, Qinghai province: Ph.D.
159
160
161
162
163
164

165
166
167
168
169 thesis, Beijing, Chinese Academy of Geological Sciences, 104p (in Chinese with English abs.).
170

171
172 Gao, Y.B., 2013, The intermediate-acid intrusive magmatism and mineralization in Oimantag, East Kunlun Mountains: Ph.D. thesis, Xi'an,
173
174 Chang'an University, 1-245p (in Chinese with English abs.).
175

176
177 Gao, Y.B., Li, W.Y., Qian, B., Li, K., Li, D.S., He, S.Y., Zhang, Z.W., Zhang, J.W., 2014, Geochronology, geochemistry and Hf isotopic
178
179 compositions of the granitic rocks related with iron mineralization in Yemaquan deposit, East Kunlun, NW China: *Acta Petrologica Sinica*, v.
180
181 30, p. 1647-1665 (in Chinese with English abs.).
182
183

184
185 Guo, T.Z., Liu, R., Chen, F.B., Bai, X.D., Li, H.G., 2011, LA-MC-ICPMS zircon U-Pb dating of Wulanwuzhuer porphyritic syenite granite in
186
187 the Qimantag Mountain of Qinghai and its geological significance: *Geological Bulletin of China*, v. 30, p. 1203-1211 (in Chinese with
188
189 English abs.).
190

191
192 He, C., 2015, Geological characteristics, genesis and geological significance of granite intrusion in Halasen area, Qinghai Province: master
193
194 thesis, Wuhan, China University of Geosciences (Wuhan), 1-46p (in Chinese with English abs.).
195

196
197 Li, G.C., Feng, C.Y., Wang, R.J., Ma, S.C., Li, H.M., Zhou, A.S., 2012, SIMS zircon U-Pb age, petrochemistry and tectonic implications of
198
199 granitoids in northeastern Baiganhu W-Sn orefield, Xinjiang: *Acta Geoscientica Sinica*, v. 33, p. 216-226 (in Chinese with English abs.).
200
201
202
203
204
205

206
207
208
209
210
211
212
213
214
215
216
217
218
219
220
221
222
223
224
225
226
227
228
229
230
231
232
233
234
235
236
237
238
239
240
241
242
243
244
245
246

- Li, J.C., Kong, H.L., Su, Y.Z., Namkha, N., Jia, Q.Z., Guo, X.Z., Zhang, B., 2017, Ar-Ar age of altered sericite, zircon U-Pb age of quartz diorite and geochemistry of the Naomuhun Gold deposit, East Kunlun: *Acta Geologica Sinica*, v. 91, p. 979-991 (in Chinese with English abs.).
- Li, S.J., Sun, F.Y., Gao, Y.W., Zhao, J.W., Li, L.S., Yang, Q.A., 2012, The theoretical guidance and the practice of small intrusions forming large deposits——The enlightenment and significance for searching breakthrough of Cu-Ni sulfide Deposit in Xiarihamu, East Kunlun, Qinghai: *Northwestern Geology*, v. 45, p. 185-191 (in Chinese with English abs.).
- Li, X., Yuan, W.M., Hao, N.N., Duan, H.W., Chen, X.N., Mo, X.X., Zhang, A.K., 2014, Characteristics and tectonic setting of granite in Wulonggou area, East Kunlun Mountains: *Global Geology*, v. 33, p. 275-288 (in Chinese with English abs.).
- Liu, B., Ma, C.Q., Guo, P., Zhang, J.Y., Xing, F.H., Huang, J., Jiang, H.A., 2013, Discovery of the Middle Devonian A-type granite from the Eastern Kunlun Orogen and its tectonic implications: *Earth Science-Journal of China University of Geosciences*, v. 38, p. 947-962 (in Chinese with English abs.).
- Liu, B., Ma, C.Q., Zhang, J.Y., Xiong, F.H., Huang, J., Jiang, H.A., 2012, Petrogenesis of Early Devonian intrusive rocks in the east part of Eastern Kunlun Orogen and implication for Early Palaeozoic orogenic processes: *Acta Petrologica Sinica*, v. 28, p. 1785-1807 (in Chinese

247
248
249
250
251 with English abs.).
252
253

254 Liu, Y.H., Liu, H.L., Huang, S.F., Gao, H.X., Zhang, Y.Q., Li, Z.G., Zheng, X.Z., 2011, Metallogenic epoch and geological features of Suishizi
255 porphyry gold deposit in Liziyuan area, west Qinling mountain: *Gold*, v. 32, p. 12-18 (in Chinese with English abs.).
256
257

258
259 Liu, Z.Q., Pei, X.Z., Li, R.B., Li, Z.C., Zhang, X.F., Liu, Z.G., Chen, G.C., Chen, Y.X., Ding, S.P., Guo, J.F., 2011, LA-ICP-MS zircon U-Pb
260 geochronology of the two suites of ophiolites at the Buqingshan area of the A'nyemaqen Orogenic Belt in the southern margin of East
261 Kunlun and its tectonic implication: *Acta Geologica Sinica*, v. 85, p. 185-194 (in Chinese with English abs.).
262
263
264

265
266 Mao, J.W., Zhang, Z.H., Yang, J.M., Wang, Z.L., 2000, Fluid inclusions of shear zone type gold deposits in the western part of North Qilian
267 Mountain: *Mineral Deposits*, v. 19, p. 9-16 (in Chinese with English abs.).
268
269

270
271 Qi, J.Z., Li, L., Yuan, S.S., Liu, Z.J., Liu, D.Y., Wang, Y.B., Li, Z.H., 2005, A SHRIMP U-Pb chronological study of zircons from quartz veins
272 of Yangshan gold deposit, Gansu Province: *Mineral Deposits*, v. 24, p. 141-150 (in Chinese with English abs.).
273
274

275
276 Qi, S.S., Deng, J.F., Ye, Z.F., Liu, R., Wang, G.L., 2013, LA-ICP-MS zircon U-Pb dating of Late Devonian diabase dike swarms in Qimantag
277 area: *Geological Bulletin of China*, v. 32, p. 1385-1393 (in Chinese with English abs.).
278
279

280
281 Shao, S.C., Wang, D.B., 2001, ^{39}Ar - ^{40}Ar dating of the three typical gold deposits and its geological significance in the southern Qinling region:
282
283
284
285
286
287

288
289
290
291
292
293
294
295
296
297
298
299
300
301
302
303
304
305
306
307
308
309
310
311
312
313
314
315
316
317
318
319
320
321
322
323
324
325
326
327
328

Acta Geologica Sinica, v. 75, p. 106-110 (in Chinese with English abs.).

Tian, G.K., Meng, F.C., Fan, Y.Z., Liu, Q., Duan, X.P., 2016, The characteristics of Early Paleozoic post-orogenic granite in the East Kunlun orogen: A case study of Dagangou granite: Acta Petrologica et Mineralogica, v. 35, p. 371-390 (in Chinese with English abs.).

Wang, G., Sun, F.Y., Li, B.Y., Li, S.J., Zhao, J.W., Yang, Q.A., Ao, Z., 2013, Zircon U-Pb geochronology and geochemistry of the Early Devonian syenogranite in the Xiarihamu ore district from East Kunlun, with Implications for the geodynamic setting: Geotectonica et Metallogenia, v. 37, p. 685-697 (in Chinese with English abs.).

Wang, T., 2015, Study of the geological characteristics and genesis of Wulonggou gold deposit, Qinghai province: master thesis, China University of Geosciences (Beijing), 84p (in Chinese with English abs.).

Wu, S.P., Wu, C.L., Chen, Q.L., 2007, Characteristics and tectonic setting of the Tula aluminous A-type granite at the south side of the Altyn Tagh fault, NW China: Geological Bulletin of China, v. 26, p. 1385-1392 (in Chinese with English abs.).

Xi, R.G., Xiao, P.X., Wu, Y.Z., Dong, Z.C., Guo, L., Gao, X.F., 2010, The geological significances, composition and age of the monzonitic granite in Kendekeke iron mine: Northwestern Geology, v. 43, p. 195-202 (in Chinese with English abs.).

Xiao, Y., Feng, C.Y., Li, D.X., Liu, J.N., 2014, Chronology and fluid inclusions of the Guoluolongwa gold deposit in Qinghai province: Acta

329
330
331
332
333 Geologica Sinica, v. 88, p. 895-902 (in Chinese with English abs.).
334

335
336 Xiong, F.H., 2014, Spatial-temporal pattern, petrogenesis and geological implications of Paleo-Tethyan granitoids in the East Kunlun Orogenic
337
338 belt (eastern segment): Ph.D. thesis, Wuhan, China University of Geosciences, 1-191p (in Chinese with English abs.).
339

340
341 Yan, W., Qiu, D.M., Ding, Q.F., Liu, F., 2016, Geochronology, petrogenesis, source and its structural significance of Houtougou monzogranite
342
343 of Wulonggou area in Eastern Kunlun Orogen: Journal of Jilin University (Earth Science Edition), v. 46, p. 443-460 (in Chinese with
344
345 English abs.).
346
347

348
349 Yang, J.G., Yang, L.H., Ren, Y.X., Li, Z.P., Song, Z.B., 2005, Isotopic Geochronology of the ore-forming process in the Hanshan gold deposit
350
351 of the North Qilian Mountains: Acta Geoscientica Sinica, v. 26, p. 315-320 (in Chinese with English abs.).
352

353
354 Yin, L.J., Liu, H.J., Yang, L.G., Liu, W.M., 2013, Geochronology, geochemistry and geological significance of granites from the Baishiya skarn
355
356 iron-polymetallic deposit, Dulan, Qinghai Province: Xinjiang Geology, v. 31, p. 248-255 (in Chinese with English abs.).
357

358
359 Yue, W.H., Gao, J.G., Zhou, J.X., 2013, LA-ICP-MS Zircon U-Pb Ages and Lithogeochemistry of Basic Dykes in the Guoluolongwa gold ore
360
361 Field, Qinghai Province, China: Journal of Mineralogy and Petrology, v. 33, p. 93-102 (in Chinese with English abs.).
362

363
364 Yue, W.H., Zhou, J.X., Gao, J.G., Huang, Y.H., Jia, F.J., 2017, Geochemistry, zircon U-Pb chronology and geological implications of Sederi
365
366
367
368
369

370
371
372
373
374
375
376
377
378
379
380
381
382
383
384
385
386
387
388
389
390
391
392
393
394
395
396
397
398
399
400
401
402
403
404
405
406
407
408
409
410

diabase, Dulan county, Qinghai province: Bulletin of Mineralogy, Petrology and Geochemistry, v. 36, p. 270-278 (in Chinese with English abs.).

Zhang, D.Q., Dang, X.Y., She, H.Q., Li, D.X., Feng, C.Y., Li, J.W., 2005, Ar-Ar dating of orogenic gold deposits in northern margin of Qaidam and East Kunlun Mountains and its geological significance: Mineral Deposits, v. 24, p. 87-98 (in Chinese with English abs.).

Zhao, L.Q., Chen, X., Zhou, H., Li, X.M., 2001, Metallogenic epoch of Jinlongshan micro-fine disseminated gold deposit, south Qinlin Mountain: Chinese Journal of Geology, v. 36, p. 489 (in Chinese with English abs.).